

CHANGE-POINT DETECTION AND SUPPORT RECOVERY FOR SPATIALLY INDEXED FUNCTIONAL DATA

BY FENGYI SONG^{1,a}, DECAI LIANG^{1,b} AND CHANGLIANG ZOU^{1,c}

¹*School of Statistics and Data Science, Nankai University*, ^a*sauntbai@gmail.com*; ^b*liangdecai@nankai.edu.cn*;
^c*nk.chlzou@gmail.com*

Large volumes of spatiotemporal data, characterized by high spatial and temporal variability, may experience structural changes over time. Unlike traditional change-point problems, each sequence in this context consists of function-valued curves observed at multiple spatial locations, with typically only a small subset of locations affected. This paper addresses two key issues: detecting the global change-point and identifying the spatial support set, within a unified framework tailored to spatially indexed functional data. By leveraging a weakly separable cross-covariance structure—an extension beyond the restrictive assumption of space-time separability—we incorporate functional principal component analysis into the change-detection methodology, while preserving common temporal features across locations. A kernel-based test statistic is further developed to integrate spatial clustering pattern into the detection process, and its local variant, combined with the estimated change-point, is employed to identify the subset of locations contributing to the mean shifts. To control the false discovery rate in multiple testing, we introduce a functional symmetrized data aggregation approach that does not rely on pointwise p -values and effectively pools spatial information. We establish the asymptotic validity of the proposed change detection and support recovery method under mild regularity conditions. The efficacy of our approach is demonstrated through simulations, with its practical usefulness illustrated in an application to China’s precipitation data.

1. Introduction.

1.1. *Motivation and Background.* With the rapid advancement of technology, large-scale spatiotemporal data at high frequencies are increasingly available in many fields, such as ecology, epidemiology, and environmental science (e.g., [Cressie and Wikle, 2011](#); [Liu, Ray and Hooker, 2017](#); [Yan, Paynabar and Shi, 2018](#)). Motivated by an empirical analysis of China’s precipitation data in Section 6, we investigate the change detection of annual patterns over a spatial region, followed by the support recovery of locations where these changes occur. Suppose that for each year i , we observe precipitation data $X_i(\mathbf{s}_j; t)$ across times $t \in \mathcal{T}$ at spatial locations $\mathbf{s}_j \in \mathcal{S}$. Our first concern is the following change-point model:

$$X_i(\mathbf{s}_j; t) = \begin{cases} \mu_0^*(\mathbf{s}_j; t) + \varepsilon_i(\mathbf{s}_j; t), & \text{for } i = 1, \dots, \tau^*; \\ \mu_1^*(\mathbf{s}_j; t) + \varepsilon_i(\mathbf{s}_j; t), & \text{for } i = \tau^* + 1, \dots, n, \end{cases}$$

where τ^* is an unknown change point, $\mu_0^*(\cdot; \cdot)$ and $\mu_1^*(\cdot; \cdot)$ represent the spatiotemporal mean functions before and after the change, and $\varepsilon_i(\cdot; \cdot)$ is a mean-zero random field with some spatiotemporal covariance structure. After detecting a change-point, we then focus on identifying the subset of spatial locations that contribute to the change, as the number of affected

Keywords and phrases: change-point detection, false discovery rate, functional data, separable covariance structure, spatial multiple testing, spatiotemporal data.

sites is typically small relative to the entire domain. Therefore, the second goal is to identify the non-zero support set

$$\{\mathbf{s}_j \in \mathcal{S} : \mathbb{E}\{X_{\tau^*+1}(\mathbf{s}_j; \cdot) - X_{\tau^*}(\mathbf{s}_j; \cdot)\} \neq 0\},$$

while controlling the associated error rate. In particular, it is anticipated that incorporating spatial structures, such as clustering or correlation patterns, into the models could improve the efficacy of signal detection and the interpretability of scientific findings.

Functional data analysis (FDA) has received growing attention due to its effectiveness in feature extraction and dimension reduction for data observed or measured over a continuous domain. Modern scientific applications increasingly involve functional data as a basic measurement structure across diverse settings, giving rise to the so-called *second-generation functional data* (Wang, Chiou and Müller, 2016; Koner and Staicu, 2023) and the corresponding challenges in statistical inference. Taking the observed dataset in our study as an example, for each year i , the measurement $X_i(\mathbf{s}_j; \cdot)$ at location \mathbf{s}_j is treated as a functional curve across $t \in \mathcal{T}$, and the annual collection over a set of locations $\mathbf{s}_j \in \mathcal{S}$ forms replicated spatial functional curves, commonly referred to as *spatially indexed functional data*. Change-point analysis for functional data has been extensively studied in these years, with various applications for channel profile monitoring (Paynabar, Zou and Qiu, 2016), temperature shift detection (Berkes et al., 2009), and mortality rates analysis (Li, Li and Shang, 2024) etc. Most existing methodologies have been developed within the scope of univariate or dependent functional data (Hörmann et al., 2010; Aston and Kirch, 2012; Aue, Rice and Sönmez, 2018), with classical techniques—such as the cumulative sum (CUSUM) procedure—being widely adopted in combination with FDA tools (Zhang et al., 2011; Li, Li and Shang, 2024). For spatially indexed functional data, Gromenko, Kokoszka and Reimherr (2017) proposed a change detection approach for the mean function of the spatiotemporal process under the assumption of space-time separability, a well-known concept in conventional spatial statistics (e.g. Cressie and Wikle, 2011). This assumption allows the spatial and temporal covariance structure to be estimated separately, and the functional principal component analysis (FPCA) can then be exploited to depict the temporal pattern.

Our second objective—the support recovery for massive spatial components—falls within the framework of spatial multiple testing, with relevant applications involving the change identification of environmental or climate fields (Sun et al., 2015), functional neuroimaging (Brown et al., 2014), and disease mapping (Gao, Banerjee and Ritz, 2023), etc. For instance, the study of weather risk attribution forecast typically covers a large number of events, namely the systematic study, instead of the targeted study that examines one single event (Risser, Paciorek and Stone, 2019), leading to simultaneous analyses on a list of events. The false discovery rate (FDR; Benjamini and Hochberg, 1995), defined as the expected fraction of false discoveries among all discoveries, has become a popular and practical criterion for large-scale hypothesis testing. While the classical Benjamini-Hochberg (BH) method has been shown to be valid for controlling the FDR under various dependence conditions, (e.g. Benjamini and Yekutieli, 2001), a variety of methods have been proposed to improve power by leveraging specific characteristics of the data at hand, such as spatial clusters or local sparsity (Pacífico et al., 2004; Cao and Wu, 2015; Yun and Bo, 2022). Recently Cai, Sun and Xia (2022) proposed an adaptive weighting p -value approach by incorporating the local sparsity structure of spatial signals, which provides a convenient and suitable tool for a wide range of spatial multiple testing problems.

1.2. *Challenges and Connections to Existing Works.* The analysis of cross-covariance structures plays a critical role in multivariate or spatial functional data, particularly in the formulation of an appropriate FPCA procedure (Paynabar, Zou and Qiu, 2016; Zhang and

Li, 2022). For change-point detection, similar approaches have been adopted by Berkes et al. (2009) for univariate functional data and generalized by Gromenko, Kokoszka and Reimherr (2017) for spatially indexed functional data based on the space-time separability, which decomposes the full covariance into a product of a purely spatial covariance and a purely temporal covariance. Though heavily used in spatial statistics, the separability assumption has been shown to be unrealistic for many real applications through hypothesis testing procedures (e.g. Aston et al., 2017). As a result, it remains both challenging and valuable to bring up more flexible and reasonable covariance structures that can serve as a valid foundation for subsequent inference tasks, such as dimension reduction and change detection.

The second challenge involves effectively integrating the spatial clustering pattern into the detection approach for massive datasets. In real-world applications, it is generally expected that a location and its adjacent neighbors are more likely to belong to similar regions, whether or not they experience changes, with nearby locations being more heavily affected than those that are spatially distant. Gromenko, Kokoszka and Reimherr (2017) proposed averaging variability across diverse locations using a spatial weighting function, but this method does not account for the clustering pattern among spatial neighborhoods. In other fields, such as large-scale sequential surveillance, research has demonstrated that aggregating local information and utilizing spatial clustering can improve the efficiency of anomaly detection (Yan, Paynabar and Shi, 2018; Ren et al., 2022). When multiple testing is performed on spatial signals, incorporating the relationships between individual locations and spatial clusters into the inferential process is also commonly recommended to increase statistical power (e.g. Benjamini and Heller, 2007; Sun et al., 2015). Although not directly applicable to our dataset, where observations at each spatial location are function-valued objectives, these insights suggest the potential for developing a more powerful procedure for detecting spatial structures of interest.

Spatial support recovery presents another challenge not typically encountered in conventional spatiotemporal statistics. While global change-point tests for entire random fields have been extensively investigated (e.g. Li, Zhang and Smerdon, 2016), it is often more appealing if one can further identify the specific subsets where changes occur. This necessitates a finite approximation strategy at the location level for inference within a continuous spatial domain, inevitably leading to issues of multiplicity or high dimensionality due to the large number of spatial sites. To control the number of incorrect rejections at an acceptable level, the FDR criterion has been widely adopted and extended to spatial signals, with many existing methods relying on a two-component mixture prior distribution for individual p -values. For example, Sun et al. (2015) proposed an oracle procedure that utilizes hyperparameter estimation to represent the posterior probability of this model, while Yun and Bo (2022) employed an EM algorithm to fit the density of p -values based on temporally stationary spatiotemporal fields. However, in the spatiotemporal context of interest, the assumption of such a pre-specified model for p -values may be questionable. Furthermore, in comparison to global change-detection procedures, accurately deriving the asymptotic properties of local test statistics that incorporate clustering information poses significant challenges, rendering a p -value-based approach less feasible. Alternatively, one may consider some p -value-free approaches, such as the knockoff filter (Barber and Candès, 2015) and the symmetrized data aggregation (SDA) approach (Du et al., 2021; Chen et al., 2023), which, to our knowledge, have not yet been adapted to the spatial multiple testing problem under consideration.

1.3. Our Contributions. In this article, we adopt a global-to-local perspective for spatially indexed functional data, addressing both change-point detection and spatial multiple testing within a unified framework.

- We leverage a weakly separable structure for spatiotemporal modeling, which offers a more flexible and empirically realistic cross-covariance configuration compared to the conventional separability assumption (e.g. [Gromenko, Kokoszka and Reimherr, 2017](#)). Building on this structure, we develop an efficient spatial FPCA procedure via a differencing covariance estimator, which preserves the structural change information and serves as the foundation for the subsequent inference tasks.
- For global change detection, we construct an asymptotically valid hypothesis testing procedure via a CUSUM procedure integrated with the above FPCA method. The change-point is then consistently estimated through a novel kernel aggregation strategy that enhances detection capability by exploiting spatial clustering patterns.
- To identify the specific locations with mean shifts, we propose a functional SDA approach based on a variant of the kernel-based statistics, ensuring valid FDR control and power improvement in multiple testing. In particular, we derived uniform convergence rates for the quantities based on the FPCA and change-point estimators, providing a cornerstone for establishing the symmetry property of our ranking statistics.
- Our method is model-free in several aspects. First, the proposed change detection procedure avoids strong structural assumptions—such as stationarity or Gaussianity—by leveraging replicated spatiotemporal observations. Second, the SDA-based multiple testing rule does not rely on the conventional two-component mixture model for location-wise p -values (e.g. [Cai, Sun and Xia, 2022](#)), resulting in a leaner framework for FDR control. Furthermore, the established theoretical guarantees hold broadly across diverse spatial sampling schemes, enhancing the method’s practical applicability.

To the best of our knowledge, this work is the first to integrate global change detection and local multiple testing within a coherent framework, providing a more appealing and comprehensive approach to spatiotemporal change-point modeling. Simulation studies demonstrate the superiority of the proposed detection procedure over existing ones in terms of finite-sample performance, and the application to China’s precipitation data further illustrates the practical utility and interpretability of our methods.

1.4. *Organization.* The rest of this article is organized as follows. In Section 2, we present the foundational change-point model for spatially indexed functional curves under the weakly separable structure. Based on the proposed FPCA estimators in Section 2.2, we develop a global change-point detection procedure, accompanied by an asymptotic investigation on the test statistics, in Section 3. This is followed by an SDA-based support recovery procedure, along with a justification of the FDR validity in Section 4. We illustrate the empirical performance of the proposed methods through a simulation study in Section 5, and a real example using China’s precipitation data in Section 6. Additional technical details and numerical results are provided in the Appendix.

1.5. *Notations.* We let $\lambda_{\min}(\mathbf{A})$ and $\lambda_{\max}(\mathbf{A})$ denote the smallest and largest eigenvalues of a square matrix \mathbf{A} , and denote $\mathbf{A}(j, k)$ as the (j, k) -th element of \mathbf{A} . For a set \mathcal{M} , let $|\mathcal{M}|$ be its cardinality. For a vector $\mathbf{x} = (x_1, \dots, x_p)^\top$, let $\|\mathbf{x}\|$ be the l_2 norm and $\|\mathbf{x}\|_\infty = \max_{j=1, \dots, p} |x_j|$ represent the l_∞ norm. Denote $\langle \cdot, \cdot \rangle_p$ as the inner product between two p -dim vector. For any two functions $f(t)$ and $g(t) \in L^2(\mathcal{T})$, where $L^2(\mathcal{T})$ denotes the space of square-integrable functions on \mathcal{T} , we denote the inner product $\langle f(\cdot), g(\cdot) \rangle_{\mathcal{T}} = \int_{\mathcal{T}} f(t)g(t)dt$ and the corresponding norm $\|f(\cdot)\|_{\mathcal{T}} = \langle f(\cdot), f(\cdot) \rangle_{\mathcal{T}}^{1/2}$.

2. The basic spatiotemporal change-point model and FPCA approach. Let $X_i(\mathbf{s}_j; t)$ be the functional observation across $t \in \mathcal{T}$ taken at the spatial location $\mathbf{s}_j \in \mathcal{S}$ on day or year

i , where \mathcal{S} and \mathcal{T} represent the spatial and time domains, respectively. In this article, we treat the temporal records across \mathcal{T} as fully observed functional data, while the spatial observations are available at discrete locations $\{\mathbf{s}_j\}_{j=1}^p$. Moreover, $X_i(\mathbf{s}_j; t)$ is observed from the latent random process $X_i(\mathbf{s}; t)$.

ASSUMPTION 2.1. The process $X_i(\mathbf{s}; t)$ is a spatiotemporal random field in $L^2(\mathcal{S} \times \mathcal{T})$, i.e. $\mathbb{E} \int_{\mathcal{S} \times \mathcal{T}} X_i^2(\mathbf{s}; t) d\mathbf{s} dt < \infty$.

Under Assumption 2.1, for each $i = 1, \dots, n$, $X_i(\mathbf{s}; t)$ can be expressed as

$$X_i(\mathbf{s}; t) = \mu_i(\mathbf{s}; t) + \varepsilon_i(\mathbf{s}; t), \quad i = 1, \dots, n,$$

where $\mu_i(\mathbf{s}; t)$ is a deterministic mean function, and $\varepsilon_i(\mathbf{s}; t)$ is a zero-mean random effect.

ASSUMPTION 2.2. Each $\mu_i(\mathbf{s}; t)$ is a smooth function on $\mathcal{S} \times \mathcal{T}$. Moreover, $\{\varepsilon_i(\mathbf{s}; t)\}_{i=1}^n$ are i.i.d spatiotemporal random fields with continuous covariance functions defined as $C(\mathbf{s}, t; \mathbf{s}', t') = \mathbb{E} \{\varepsilon_i(\mathbf{s}; t) \varepsilon_i(\mathbf{s}'; t')\}$.

Under Assumptions 2.1 to 2.2, the covariance function $C(\cdot, \cdot; \cdot, \cdot)$ can also be viewed from the perspective of operators in Hilbert-Schmidt spaces; see Appendix B.1 for more details. Considering that at some time τ^* , a change has occurred in the mean function μ_i , where we abbreviate $\mu_i(\mathbf{s}; t)$ as μ_i for simplicity. Our detection problem involves two main steps. The first step is formulated as the following hypothesis test:

(P1)

$$\mathcal{H}_0 : \mu_1 = \dots = \mu_n \text{ versus } \mathcal{H}_1 : \mu_1 = \dots = \mu_{\tau^*} \neq \mu_{\tau^*+1} = \dots = \mu_n \text{ for some } 1 \leq \tau^* < n,$$

where the equalities are in the $L^2(\mathcal{S} \times \mathcal{T})$ sense, followed by the estimation of the occurring time τ^* . In this paper, we focus on the one-change-point problem, although additional change points can be further detected using the proposed methods as needed. Additionally, the problem in (P1) implies that we are testing for a change in the mean function, under the assumption that the covariance structures remain unchanged. This approach is common in change-point detection, as allowing both the mean and variance to change can complicate the analysis, even for scalar variables (Horváth and Kokoszka, 2012).

After detecting the global change-point, the next step is to identify the spatial locations where these changes occur. Specifically, let $\mathbb{S} = \{\mathbf{s}_1, \dots, \mathbf{s}_p\}$ represent the set of discretely observed locations, and denote $\mathcal{A} = \{\mathbf{s}_j \in \mathbb{S} : \mu_{\tau^*}(\mathbf{s}_j; \cdot) \neq \mu_{\tau^*+1}(\mathbf{s}_j; \cdot)\}$ the subset of \mathbb{S} with mean changes at τ^* , where the equalities are in the $L^2(\mathcal{T})$ sense. The focus here is on detecting this breaking set in space, as it is often believed that only a subset of spatial locations contributes to the changes, meaning that $|\mathcal{A}|$ is small relative to p . One can formulate an analogous model for temporal support recovery if the data exhibit similar patterns in the time domain. Define $\theta_j = \mathbb{I}\{\mathbf{s}_j \in \mathcal{A}\}$, where \mathbb{I} is an indicator function and $\theta_j = 0/1$ corresponds to a null/nonnull variable, we consider the multiple hypothesis tests:

$$(P2) \quad \mathcal{H}_0^j : \theta_j = 0 \text{ versus } \mathcal{H}_1^j : \theta_j = 1, \text{ for } j = 1, \dots, p.$$

Let δ_j be the binary test decision at location \mathbf{s}_j , where $\delta_j = 1$ if \mathcal{H}_0^j is rejected and $\delta_j = 0$ otherwise. The false discovery proportion (FDP) and true discovery proportion (TDP) are defined as follows:

$$(1) \quad \text{FDP} = \frac{\sum_{j=1}^p (1 - \theta_j) \delta_j}{\max\{\sum_{j=1}^p \delta_j, 1\}}, \quad \text{TDP} = \frac{\sum_{j=1}^p \theta_j \delta_j}{\max\{\sum_{j=1}^p \theta_j, 1\}}.$$

Our objective is to accurately recover the informative set \mathcal{A} while controlling $\text{FDR} = \mathbb{E}(\text{FDP})$, and simultaneously achieving a high level of power, defined as $\mathbb{E}(\text{TDP})$.

2.1. *Weakly separable covariance structure.* As the covariance of spatiotemporal processes may be quite intricate, we aim to develop the methodology under some flexible covariance structure; i.e. the following concept of weak separability (Liang et al., 2023).

DEFINITION 1. A spatiotemporal process $X_i(\mathbf{s}; t)$ in $L^2(\mathcal{S} \times \mathcal{T})$ is weakly separable if there exists some orthonormal basis $\{\psi_r(\cdot)\}_{r=1}^\infty$ in $L^2(\mathcal{T})$ such that

$$(2) \quad X_i(\mathbf{s}; t) = \mu_i(\mathbf{s}, t) + \sum_{r=1}^{\infty} \xi_{ir}(\mathbf{s}) \psi_r(t)$$

holds almost surely in $L^2(\mathcal{S} \times \mathcal{T})$, where $\{\xi_{ir}(\cdot)\}_{r=1}^\infty$ are mutually uncorrelated spatial processes in $L^2(\mathcal{S})$, i.e. for any $r \neq r'$, $\text{cov}\{\xi_{ir}(\mathbf{s}), \xi_{ir'}(\mathbf{s}')\} = 0$ for any \mathbf{s} and \mathbf{s}' in \mathcal{S} .

The expansion (2) entails that $\xi_{ir}(\mathbf{s}) = \langle \varepsilon_i(\mathbf{s}; \cdot), \psi_r(\cdot) \rangle_{\mathcal{T}}$ for any $\mathbf{s} \in \mathcal{S}$. Moreover, it follows from Definition 1 that the covariance function of $X_i(\mathbf{s}; t)$ can be decomposed as

$$C(\mathbf{s}, t; \mathbf{s}', t') = \sum_{r=1}^{\infty} \sigma_r(\mathbf{s}, \mathbf{s}') \psi_r(t) \psi_r(t'),$$

where $\sigma_r(\mathbf{s}, \mathbf{s}') = \mathbb{E}\{\xi_{ir}(\mathbf{s}) \xi_{ir}(\mathbf{s}')\}$ is the r th eigenvalue of the covariance function $C_{\mathbf{s}, \mathbf{s}'(\cdot, \cdot)} = C(\mathbf{s}, \cdot; \mathbf{s}', \cdot)$, and $\psi_r(\cdot)$ is the corresponding eigenfunction. Following the common perspective of functional principal component analysis (FPCA), the model (2) generalizes the Karhunen-Loève (KL) expansion for spatial functional fields, therefore we also call $\{\psi_r(\cdot)\}_{r=1}^\infty$ and $\{\xi_{ir}(\cdot)\}_{r=1}^\infty$ as the functional principal components (FPCs) and FPC scores, respectively.

It can be seen from the definition that, the proposed weak separability generalizes the conventional concept of separability (also referred to as *strong separability* in the sequel for a more clear comparison), and provides a flexible yet parsimonious representation for the spatially indexed functional data of concern. For each spatial location \mathbf{s}_j , the observed functional process $X_i(\mathbf{s}_j; \cdot)$ can be projected onto a common basis $\{\psi_r(\cdot)\}_{r=1}^\infty$, resulting in a sequence of FPC scores $\{\xi_{ir}(\mathbf{s}_j)\}_{r=1}^\infty$. Let $\boldsymbol{\xi}_{ir} = (\xi_{ir}(\mathbf{s}_1), \dots, \xi_{ir}(\mathbf{s}_p))^T$, the weak separability implies that provided with such a basis system, $\{\boldsymbol{\xi}_{ir}\}_{r=1}^\infty$ are mutually uncorrelated for any $r \neq r'$, i.e. $\mathbb{E}\{\xi_{ir}(\mathbf{s}_j) \xi_{ir'}(\mathbf{s}_k)\} = 0$ for any $j, k = 1, \dots, p$. On the other hand, for each r , the p -variate vector $\boldsymbol{\xi}_{ir}$ may be correlated with some covariance structure

$$\sigma_r(\mathbf{s}_j, \mathbf{s}_k) = \mathbb{E}\{\xi_{ir}(\mathbf{s}_j) \xi_{ir}(\mathbf{s}_k)\}, \quad j, k = 1, \dots, p,$$

and thus can be modeled using techniques in traditional spatial or multivariate statistics. This lays the foundation for the following FPCA procedure and the testing approaches in Sections 3 and 4.

2.2. *Spatial FPCA under the change-point model.* To develop the change detection procedure for spatial functional data, we first need to estimate the eigenvalues and eigenfunctions, which relies on the proper estimation of the covariance function. Define $\mathbf{X}_i(t) = (X_i(\mathbf{s}_1; t), \dots, X_i(\mathbf{s}_p; t))^T$ and $\boldsymbol{\varepsilon}_i(t) = (\varepsilon_i(\mathbf{s}_1; t), \dots, \varepsilon_i(\mathbf{s}_p; t))^T$, both of which can be regarded as p -dim functional processes with some cross-covariance structures implied by $C(\cdot, \cdot; \cdot, \cdot)$. Under the weakly separable model (2), it can be observed that $\{\psi_r(\cdot)\}$ are, unique up to a sign, the eigenfunctions of the marginal covariance function

$$H(t, t') = \frac{1}{p} \mathbb{E} \left\{ \langle \boldsymbol{\varepsilon}_i(t), \boldsymbol{\varepsilon}_i(t') \rangle_p \right\} = \frac{1}{p} \sum_{j=1}^p C(\mathbf{s}_j, t; \mathbf{s}_j, t').$$

Moreover, the eigenbasis of $H(t, t')$ is shown to be optimal in the sense that it retains the largest amount of total variability among the p -dim vectors $\langle \mathbf{X}_i(\cdot), \psi_r(\cdot) \rangle_{\mathcal{T}}$ for any orthonormal basis $\{\tilde{\psi}_r(\cdot)\}_{r=1}^{\infty}$ (Zapata, Oh and Petersen, 2022). This motivates us to estimate $\psi_r(\cdot)$ based on the eigendecomposition of an estimator of $H(\cdot, \cdot)$. For this purpose, a naive approach may be performed based on $\tilde{H}(t, t') = p^{-1} \sum_{j=1}^p \tilde{C}_{jj}(t, t')$, where $\tilde{C}_{jj}(t, t') = n^{-1} \sum_{i=1}^n \{X_i(\mathbf{s}_j; t) - \bar{X}_j(t)\} \{X_i(\mathbf{s}_j; t') - \bar{X}_j(t')\}$ is the sample covariance function of $X(\mathbf{s}_j; \cdot)$ and $\bar{X}_j(t) = n^{-1} \sum_{i=1}^n X_i(\mathbf{s}_j; t)$. However, under the alternative hypothesis in (P1), such an estimated covariance function may be inconsistent due to the bias in the sample mean estimates. To address this issue, we consider the marginal covariance estimator via differencing (Paynabar, Zou and Qiu, 2016), say

$$(3) \quad \hat{H}(t, t') = \frac{1}{2p(n-1)} \sum_{i=1}^{n-1} \langle \{\mathbf{X}_{i+1}(t) - \mathbf{X}_i(t)\}, \{\mathbf{X}_{i+1}(t') - \mathbf{X}_i(t')\} \rangle_p,$$

following a similar spirit as the typical robust estimation for the covariance matrix. We will show in the proof of Theorem 2.1 that $\hat{H}(\cdot, \cdot)$ is a consistent estimator of $H(\cdot, \cdot)$ under both \mathcal{H}_0 and \mathcal{H}_1 in (P1).

Based on the above marginal covariance estimators, we then obtain the estimates $\{\hat{\lambda}_r, \hat{\psi}_r(\cdot)\}$ as the eigenvalues and eigenfunctions of $\hat{H}(\cdot, \cdot)$. One can see from Theorem 2.1 that $\hat{\psi}_r(\cdot)$ and $\hat{\lambda}_r$ are respectively consistent to $\psi_r(\cdot)$ and $\lambda_r := p^{-1} \sum_{j=1}^p \lambda_{r,j}$, where $\lambda_{r,j} := \mathbb{E}\{\xi_{ir}^2(\mathbf{s}_j)\}$ reflects the heteroskedasticity across different locations $\{\mathbf{s}_j\}_{j=1}^p$. Besides the functional components that depict the temporal variation, we propose to estimate the cross spatial covariance $\sigma_r(\mathbf{s}_j, \mathbf{s}_k)$, i.e., the $p \times p$ cross-covariance matrix $\Sigma_r = (\sigma_r(\mathbf{s}_j, \mathbf{s}_k))_{j,k=1,\dots,p}$, by

$$(4) \quad \hat{\Sigma}_r = \frac{1}{2(n-1)} \sum_{i=1}^{n-1} \left\langle \{\mathbf{X}_{i+1}(\cdot) - \mathbf{X}_i(\cdot)\}, \hat{\psi}_r(\cdot) \right\rangle_{\mathcal{T}} \left\langle \{\mathbf{X}_{i+1}(\cdot) - \mathbf{X}_i(\cdot)\}, \hat{\psi}_r(\cdot) \right\rangle_{\mathcal{T}}^T,$$

of which the off-diagonal element $\hat{\Sigma}_r(j, k)$ and diagonal element $\hat{\lambda}_{r,j} := \hat{\Sigma}_r(j, j)$ yield the cross-covariance and variance estimates respectively for $\sigma_r(\mathbf{s}_j, \mathbf{s}_k)$ and $\lambda_{r,j}$. Moreover, define the spatial correlation $\rho_r(\mathbf{s}_j, \mathbf{s}_k) = \sigma_r(\mathbf{s}_j, \mathbf{s}_k) / \sqrt{\lambda_{r,j} \lambda_{r,k}}$, we propose the corresponding estimator $\hat{\rho}_r(\mathbf{s}_j, \mathbf{s}_k) = \hat{\Sigma}_r(j, k) / \sqrt{\hat{\Sigma}_r(j, j) \hat{\Sigma}_r(k, k)}$. The convergence results for the developed FPCA estimators are established in Theorem 2.1.

ASSUMPTION 2.3. (Moments) The multivariate functional process $\boldsymbol{\varepsilon}_i(\cdot)$ satisfies that for each $j = 1, \dots, p$, $\mathbb{E}\|\boldsymbol{\varepsilon}_i(\mathbf{s}_j; \cdot)\|_{\mathcal{T}}^4 < \infty$ (which means $\mathbb{E}\{\int_{\mathcal{T}} \boldsymbol{\varepsilon}_i^2(\mathbf{s}_j; t) dt\}^2 < \infty$).

ASSUMPTION 2.4. (Eigen-gaps) For some integer $R > 0$, the eigenvalues $\{\lambda_r\}$ satisfy $\lambda_1 > \lambda_2 > \dots > \lambda_R > 0$. Moreover, there exist constants $c_1, c_2 > 0$ such that for each $1 \leq r \leq R$, $c_1 \leq \lambda_{\min}(\Sigma_r) < \lambda_{\max}(\Sigma_r) \leq c_2$.

Assumption 2.3 is a standard moment assumption for the weak convergence of (cross) covariance operators in Hilbert-Schmidt spaces (e.g. Bosq, 2000; Hsing and Eubank, 2015). Assumption 2.4 states the distinctness of the eigenvalues, which is common in FDA and ensures the consistency of eigen-estimators in Theorem 2.1. Without loss of generality, the eigendecompositions of \hat{H} and H are ordered in terms of the decreasing value of $\{\hat{\lambda}_r\}$ and $\{\lambda_r\}$ in what follows, thereby the expansion of (2) is ordered in the same way. Assumption 2.4 also implies that each of Σ_r is positive definite.

THEOREM 2.1. *Suppose that the spatiotemporal process $X_i(\cdot; \cdot)$ is weakly separable under Assumptions 2.1–2.4. Then for each $1 \leq r \leq R$ and as $n \rightarrow \infty$, we have*

$$\hat{\lambda}_r \xrightarrow{p} \lambda_r, \quad \hat{\psi}_r(\cdot) \xrightarrow{p} \psi_r(\cdot), \quad \hat{\Sigma}_r \xrightarrow{p} \Sigma_r,$$

where $\hat{\psi}_r(\cdot) \xrightarrow{p} \psi_r(\cdot)$ means $\|\hat{\psi}_r(\cdot) - \psi_r(\cdot)\|_{\mathcal{T}} = o_p(1)$, and $\hat{\Sigma}_r \xrightarrow{p} \Sigma_r$ means the element-wise convergence of $\hat{\Sigma}_r$ in probability.

Theorem 2.1 establishes the consistency of the FPCA estimator resulting from the covariance estimator $\hat{H}(\cdot, \cdot)$. Notably, the convergence results hold under both the null and alternative hypotheses in (P1). In Appendix B.1 we provide a more precise convergence rate for $\hat{\psi}_r(\cdot)$, showing that $\|\hat{\psi}_r(\cdot) - \psi_r(\cdot)\|_{\mathcal{T}} = O_p(n^{-1/2})$. Furthermore, when the dependency among the covariance functions at different locations is negligible, the convergence rate improves to $\|\hat{\psi}_r(\cdot) - \psi_r(\cdot)\|_{\mathcal{T}} = O_p((pn)^{-1/2})$. This result suggests that the estimation errors decrease as the number of locations p increases, indicating that estimation efficiency is enhanced by pooling information across different locations, benefiting from the weakly separable structure.

3. Change-point detection based on FPCA. Building on the FPCA estimators developed in Section 2.2, we propose a change-point detection method tailored for the spatially indexed functional data under study. In this section, we focus first on the scenario where the number of locations p is fixed, as the primary objective is to test for a global change-point across all locations.

3.1. Test statistics and null distribution. Recall that at each location \mathbf{s}_j , we observe the functional objects $X_i(\mathbf{s}_j; \cdot)$ across $i = 1, \dots, n$. To formulate the change-point model, for any $1 \leq \tau < n$, we define the standardized CUSUM difference:

$$\hat{\Delta}_\tau(\mathbf{s}_j; \cdot) = \frac{1}{\sqrt{n}} \left\{ \sum_{i=1}^{\tau} X_i(\mathbf{s}_j; \cdot) - \frac{\tau}{n} \sum_{i=1}^n X_i(\mathbf{s}_j; \cdot) \right\},$$

where we observe that

$$\sum_{i=1}^{\tau} X_i(\mathbf{s}_j; \cdot) - \frac{\tau}{n} \sum_{i=1}^n X_i(\mathbf{s}_j; \cdot) = \frac{\tau(n-\tau)}{n} \left\{ \frac{1}{\tau} \sum_{i=1}^{\tau} X_i(\mathbf{s}_j; \cdot) - \frac{1}{(n-\tau)} \sum_{i=\tau+1}^n X_i(\mathbf{s}_j; \cdot) \right\}.$$

Treating $\hat{\Delta}_\tau(\mathbf{s}_j; \cdot)$ as an element in $L^2(\mathcal{T})$, we then project it onto the FPCs for $r = 1, \dots, R$, yielding the scaled statistics

$$(5) \quad \hat{\eta}_{\tau,r}(\mathbf{s}_j) = \hat{\lambda}_{r,j}^{-1/2} \left\langle \hat{\Delta}_\tau(\mathbf{s}_j; \cdot), \hat{\psi}_r(\cdot) \right\rangle_{\mathcal{T}},$$

where $\hat{\lambda}_{r,j}$ and $\hat{\psi}_r(\cdot)$ are the consistent FPCA estimates obtained from the procedure in Section 2.2. By utilizing this dimension-reduction technique, we can evaluate the functional elements $\hat{\Delta}_\tau(\mathbf{s}_j; \cdot)$ through the aggregation of the first few components of $\{\hat{\eta}_{\tau,r}(\mathbf{s}_j)\}_{r=1}^{\infty}$, say $\sum_{r=1}^R \hat{\eta}_{\tau,r}(\mathbf{s}_j)$, which captures a substantial portion of the variability in $\hat{\Delta}_\tau(\mathbf{s}_j; \cdot)$, owing to the weak separability property.

As is typically observed for spatial signals, a location and its adjacent neighbors are more likely to fall in a similar type of region, either occurring changes or not. Meanwhile, the number of spatial locations affected by an abrupt break is usually not large. To incorporate

this local clustering pattern among functional curves into the change-detection approach, we proposed the following kernel-based statistic:

$$(6) \quad \hat{\eta}_{\tau,r}^{(h)} = \sum_{1 \leq j, k \leq p} K_h(\mathbf{s}_j - \mathbf{s}_k) \hat{\eta}_{\tau,r}(\mathbf{s}_j) \hat{\eta}_{\tau,r}(\mathbf{s}_k),$$

where $K_h(\cdot) = K(\cdot/h)/h^2$, with $h > 0$ representing a bandwidth that depends on the spatial observations. Here $K(\cdot)$ is a nonnegative, symmetric and bounded kernel function from \mathbb{R}^2 , which integrates to 1 and has bounded derivatives. From the perspective of nonparametric regression, this approach measures the quantity $\mathbb{E}_{\mathbf{s}}\{\mathbb{E}(\hat{\eta}_{\tau,r}^2|\mathbf{s})\}$ where $\mathbb{E}_{\mathbf{s}}$ represents the expectation with respect to some sampling density $f_{\mathbf{s}}$ of the spatial points $\mathbf{s} \in \mathbb{S}$, and $\mathbb{E}(\hat{\eta}_{\tau,r}^2|\mathbf{s})$ denotes the expectation of $\mathbb{E}\{\hat{\eta}_{\tau,r}^2(\mathbf{s})\}$ conditional on \mathbf{s} (Ren et al., 2022). The kernel statistic (6) can be viewed as employing this approach by utilizing a uniform sampling density for all spatial points. Rather than relying solely on the statistic at \mathbf{s}_j , it aggregates the quantity (5) from neighboring locations around \mathbf{s}_j , thereby enhancing signal detection capabilities by pooling information from adjacent areas.

By aggregating the statistic (6) across different FPC directions, we define $Q_h(\tau) = \sum_{r=1}^R \hat{\eta}_{\tau,r}^{(h)}$. The test statistic can then be constructed as follows:

$$(7) \quad Q_h^{max} = \max_{1 \leq \tau < n} Q_h(\tau), \quad \text{or} \quad Q_h^{sum} = \frac{1}{n} \sum_{1 \leq \tau < n} Q_h(\tau).$$

The change-point test can be conducted using either Q_h^{max} or Q_h^{sum} , which can be respectively regarded as the Kolmogorov-Smirnov or Cramér-von Mises type of functionals based on the functional cumulative sum process. Gromenko, Kokoszka and Reimherr (2017) noted that the convergence rate for Kolmogorov-Smirnov-type statistics may be slow, and therefore focused on the latter approach. By contrast, Paynabar, Zou and Qiu (2016) proposed using a simulation-based approach to approximate the distribution of the ‘‘max’’ statistic. In this paper, we focus on both the ‘‘max’’ and ‘‘sum’’ statistics, presenting their asymptotic null distribution in Theorem 3.1, and investigating their numerical performance via simulation in Section 5.

THEOREM 3.1. *Under the assumptions in Theorem 2.1 and the null hypothesis \mathcal{H}_0 in (P1),*

$$(8) \quad Q_h^{max} \xrightarrow{d} \sup_{0 < x < 1} \sum_{r=1}^R \mathbf{B}_r^\top(x) \mathbf{K}_h \mathbf{B}_r(x), \quad Q_h^{sum} \xrightarrow{d} \sum_{r=1}^R \int_0^1 \mathbf{B}_r^\top(x) \mathbf{K}_h \mathbf{B}_r(x) dx,$$

where $\mathbf{K}_h = (K_h(\mathbf{s}_j - \mathbf{s}_k))_{j,k=1,\dots,p}$ is the $p \times p$ kernel matrix, $\mathbf{B}_r(\cdot) = \{B_{1r}(\cdot), \dots, B_{pr}(\cdot)\}^\top$ are p -dimensional Brownian bridges with covariance matrix $\mathbf{P}_r = (\rho_r(\mathbf{s}_j, \mathbf{s}_k))_{j,k=1,\dots,p}$, i.e. $\mathbf{P}_r^{-1/2} \mathbf{B}_r(\cdot)$ is a vector of independent standard Brownian bridges.

REMARK 1. The convergence properties in Theorem 3.1 hold when the number of locations p is fixed, regardless of the shape or sampling scheme of the spatial domain. This contrasts with typical requirements for modeling spatiotemporal data without replicates, where consistent estimators often necessitate specific asymptotic regimes such as increasing-domain asymptotics. Given the availability of realizations for $\mathbf{X}_i(\cdot)$ across $i = 1, \dots, n$, the results in (8) also appear to be independent of the strength of spatial dependence. However, as is well-acknowledged in multivariate change-detection literature (e.g. Wang and Feng, 2023), the (second-order) correlation among different elements can not be too strong for identifying the mean breaks. This phenomenon is similarly observed in our spatiotemporal setup, where

the convergence in (8) tends to be slow if the spatial correlation is too strong. Our simulation results indicate that the proposed detection procedure performs well under a range of scenarios with moderate spatial dependency.

To approximate the quantiles of the asymptotic distribution on the right-hand side of (8), one can compute the Monte Carlo distribution based on multivariate Brownian bridges with the covariance structure \mathbf{P}_r . A typical approach involves incorporating spatial correlation estimates $\hat{\rho}_r(\cdot, \cdot)$, as provided in Section 2.2, to obtain the corresponding $\hat{\mathbf{P}}_r$. Alternatively, if the spatial correlation can be further assumed to be stationary and isotropic, as is common in spatial statistics, \mathbf{P}_r can be estimated through some smoothing procedures. For example, assuming $\rho_r(\cdot)$ is a univariate correlation function that depends only on pairwise distances, one can employ a nonparametric regression approach on the observations $\{\tilde{d}, \hat{\rho}_r(\tilde{d})\}$, where $\hat{\rho}_r(\tilde{d}) = \hat{\rho}_r(\mathbf{s}_j, \mathbf{s}_k)$, and $\tilde{d} = \|\mathbf{s}_j - \mathbf{s}_k\|$ denotes the distance between locations \mathbf{s}_j and \mathbf{s}_k . Following Gromenko, Kokoszka and Reimherr (2017), we use B-splines to obtain a nonparametric estimator $\hat{\rho}_r(\cdot)$ and consequently the matrix $\hat{\mathbf{P}}_r$, by plugging $\hat{\rho}_r(\cdot)$. Note that this approach allows for varying variances across different locations, providing a more general framework than the typical assumption of spatial stationarity.

3.2. The proposed change-detection procedure. Despite the null distribution presented in Theorem 3.1, our primary interest lies in detecting the change-point τ^* , specifically understanding the behavior of the test under the alternative hypothesis. As is typical in change-point detection, we assume that $\lim_{n \rightarrow \infty} \tau^*/n = \theta_0 \in (0, 1)$. According to Theorem 3.1, a large value of $Q_h(\tau)$ exceeding a certain threshold would suggest rejecting the null hypothesis. Define that $\mathbf{\Delta}(\cdot) = \{\Delta(\mathbf{s}_1; \cdot), \dots, \Delta(\mathbf{s}_p; \cdot)\}^T$, where $\Delta(\mathbf{s}_j; \cdot) = \mu_{\tau^*+1}(\mathbf{s}_j; \cdot) - \mu_{\tau^*}(\mathbf{s}_j; \cdot)$ denotes the functional process of the mean shift at location \mathbf{s}_j . The following theorem establishes the rate of divergence for the test statistics under the alternative.

THEOREM 3.2. *Under the assumptions in Theorem 2.1 and the alternative \mathcal{H}_1 in (P1), if there exists at least one $r = 1, \dots, R$ such that $\mathbf{\Delta}_r := \langle \mathbf{\Delta}(\cdot), \psi_r(\cdot) \rangle_{\mathcal{T}} \neq 0$, then $n^{-1}Q_h^{max} = O_p(1)$ and $n^{-1}Q_h^{sum} = O_p(1)$, with the explicit formulas for $O_p(1)$ provided in (32) of Appendix.*

Theorem 3.2 demonstrates that the developed tests are consistent provided the change is not orthogonal to the subspace spanned by the eigenfunctions. Notably, the established n -rate of divergence for Q_h^{max} and Q_h^{sum} remains valid when $p \rightarrow \infty$, since the consistency of the proposed FPCA estimators is unaffected by the dimension of p . Upon rejection of the null hypothesis, the change-point can be estimated by

$$(9) \quad \hat{\tau} = \arg \max_{1 \leq \tau < n} Q_h(\tau).$$

COROLLARY 3.1. *Under the assumptions in Theorem 3.2, we have $|\hat{\tau} - \tau^*| = O_p(1)$.*

To implement the change-point test based on the derived methodology, selecting an appropriate bandwidth h for the statistic Q_h^{max} or Q_h^{sum} is crucial. While the weak convergence results in (8) hold for any $h > 0$ theoretically (for a fixed p), the convergence rate generally improves when h is smaller. On the other hand, choosing a relatively large h may incorporate more non-zero components in $\mathbf{\Delta}_r$, enhancing the power of the test by capturing broader spatial signals. These considerations suggest that the test can perform well across a reasonable range of h . From a data-driven perspective, we propose to determine the bandwidth by first fitting a pilot model for the correlation function $\rho(\cdot)$. This can be estimated by averaging the

nonparametric estimates $\hat{\rho}_r(\cdot)$ across different components r . The bandwidth h can then be selected based on the range parameter of the fitted spatial correlation or by identifying the minimum distance at which the fitted correlation drops below a threshold ϱ . The rationale behind this approach is that neighboring locations with relatively strong dependence are more likely to belong to the informative set of signals. Additionally, it is expected that the resulting change-point will be consistent across various values of ϱ .

Another important implementation issue is the selection of the truncation number R for the eigenfunctions. It is well recognized in FDA that, the chosen parameter \hat{R} should not be too large, as this can lead to increasingly unstable FPC estimates. On the other hand, as indicated by Theorem 3.2, an excessively small \hat{R} may fail to capture sufficient signals across the components Δ_r , thereby reducing the ability to detect changes. To provide practical guideline, we adopt the fraction of variance explained (FVE) criterion, defined in our setting as

$$\text{FVE}(R) = \left(\sum_{r=1}^R \hat{\lambda}_r \right) / \left(\sum_{r=1}^{\infty} \hat{\lambda}_r \right),$$

where $\{\hat{\lambda}_r\}$ are the estimated eigenvalues from Section 2.2. Common thresholds for FVE include 80%, 90% or 95%, though our simulation results suggest that the proposed method remains robust across a wide range of FVE values.

Algorithm 1 The detection procedure for the global change-point

- 1: Conduct the FPCA procedure in Section 2.2, and
 - obtain the FPCs $\{\hat{\psi}_r(\cdot)\}$ using $\hat{H}(\cdot, \cdot)$ as defined in (3).
 - calculate the covariance matrix $\hat{\Sigma}_r$ by (4) with the corresponding correlation matrix \hat{P}_r .
- 2: Determine the truncation number \hat{R} according to a pre-specified FVE level.
- 3: Fit a nonparametric correlation function $\hat{\rho}(\cdot)$ based on \hat{P}_r , and select the bandwidth by $h = \inf\{d > 0 : \hat{\rho}(d) < \varrho\}$ for a specified ϱ . Then calculate the kernel matrix \mathbf{K}_h .
- 4: For each $\tau = 1, \dots, n$,

- obtain $\hat{\eta}_{\tau,r}(\mathbf{s}_j)$ based on the FPC estimates by (5) across $r = 1, \dots, \hat{R}$ for each \mathbf{s}_j .
- calculate the quadratic form $\hat{\eta}_{\tau,r}^{(h)} = \hat{\eta}_{\tau,r}^T \mathbf{K}_h \hat{\eta}_{\tau,r}$ with $\hat{\eta}_{\tau,r} = \{\hat{\eta}_{\tau,r}(\mathbf{s}_1), \dots, \hat{\eta}_{\tau,r}(\mathbf{s}_p)\}^T$.

Then calculate the statistic Q_h^{max} or Q_h^{sum} by (7) based on $Q_h(\tau) = \sum_{r=1}^{\hat{R}} \hat{\eta}_{\tau,r}^{(h)}$.

- 5: For each $r = 1, \dots, \hat{R}$ and $0 < x < 1$, generate the Monte Carlo samples of $\tilde{\mathbf{B}}_r(x) = \hat{P}_r^{1/2} \mathbf{B}_r^*(x)$, where $\mathbf{B}_r^*(x) = \{B_{1r}^*(x), \dots, B_{pr}^*(x)\}^T$ is a standard p -dimensional Brownian bridge. Then calculate the samples of

$$\tilde{F}_{Q_h}(x) = \sum_{r=1}^{\hat{R}} \tilde{\mathbf{B}}_r^T(x) \mathbf{K}_h \tilde{\mathbf{B}}_r(x).$$

- For the test statistic Q_h^{max} , obtain the p -value by using the Monte Carlo distribution of $\sup_{0 < x < 1} \tilde{F}_{Q_h}(x)$. Conduct the test similarly for Q_h^{sum} .

- 6: When the test is rejected, plot the function $Q_h(\tau)$ and obtain the change-point $\hat{\tau}$ by (9).
-

We illustrate the proposed change-point detection procedure in Algorithm 1. It is noteworthy that valid change-point detection can also be performed using the non-kernel statistics

$$Q_0^{max} = \max_{1 \leq \tau < n} Q_0(\tau) \text{ or } Q_0^{sum} = n^{-1} \sum_{1 \leq \tau < n} Q_0(\tau),$$

where $Q_0(\tau) = \sum_{r=1}^{\hat{R}} \sum_{j=1}^p \hat{\eta}_{\tau,r}^2(\mathbf{s}_j)$ defines the statistic $Q_h(\tau)$ for $h = 0$. This procedure employs the conventional sum of squares approach, whereas the test statistic Q_0^{sum} coincides with the statistic $\hat{\Lambda}_1$ proposed by [Gromenko, Kokoszka and Reimherr \(2017\)](#) under uniform weighting across all locations. It is important to note that $\hat{\Lambda}_1$ is derived under the assumption of strong separability. In contrast, the proposed test based on Q_h efficiently incorporates the spatial clustering information through a kernel approach, resulting in a substantial increase in power. We compare the empirical test performance of Q_h , Q_0 and those proposed by [Gromenko, Kokoszka and Reimherr \(2017\)](#) through the simulation study in Section 5.

4. Support recovery based on sample splitting. After detecting the change-point using the procedure described in Algorithm 1, the next objective is to develop a valid support recovery method for the problem (P2). A natural approach is to utilize the statistic in (5) with the estimated change-point $\hat{\tau}$, followed by calculating the p -values for all locations, denoted as $\{p_j; j = 1, \dots, p\}$, and then applying a multiple testing procedure, such as the BH procedure or the LAWS method proposed by [Cai, Sun and Xia \(2022\)](#). The LAWS method incorporates local weights for the point-wise p -values by assuming that each location has a prior probability of being an alternative, say $\pi(\mathbf{s}_j) = \Pr(\theta_j = 1)$. However, for the spatial sampling scheme under consideration, this assumption may be questionable. To address this limitation, we propose a p -value-free procedure that adaptively and effectively leverages the spatial structure, based on a combination of the proposed FPCA method and the SDA approach in [Du et al. \(2021\)](#).

4.1. *Construction of ranking statistics and FDR thresholding.* The SDA method involves constructing a series of ranking statistics with global symmetry property through sample splitting, followed by selecting a data-driven threshold to control the FDR. Adhering to this framework, we first partition the dataset into two subsets, both used to construct statistics that evaluate the evidence against null hypothesis. Specifically, we adopt an order-preserved sample-splitting approach by dividing the full sample $\mathcal{X} = \{\mathbf{X}_i(\cdot) : i = 1, \dots, n\}$ into

$$(10) \quad \mathcal{X}_O := \{\mathbf{X}_{2i-1}(\cdot) : i = 1, \dots, m\} \text{ and } \mathcal{X}_E := \{\mathbf{X}_{2i}(\cdot) : i = 1, \dots, m\},$$

where we assume that n is even for convenience. As suggested by [Chen et al. \(2023\)](#), this splitting strategy helps preserve the original change-point structure with minimal variation between the training and validation samples. The statistics on \mathcal{X}_O are constructed using (5) with the estimated change-point $\hat{\tau}$, denoted as $\hat{\eta}_{\hat{\tau},r}^O(\mathbf{s}_j)$ for $j = 1, \dots, p$; while for \mathcal{X}_E , we propose the kernel-weighted statistic:

$$(11) \quad \tilde{\eta}_{\hat{\tau},r}(\mathbf{s}_j) = \frac{\sum_k K_h(\mathbf{s}_k - \mathbf{s}_j) \hat{\eta}_{\hat{\tau},r}(\mathbf{s}_k)}{\sum_k K_h(\mathbf{s}_k - \mathbf{s}_j)},$$

where $K_h(\cdot)$ is the kernel function as defined in (6). Following a similar spirit to (6), this statistic aggregates information from the neighboring locations of \mathbf{s}_j , resulting in enhanced signals at each spatial point. The corresponding statistic calculated using the sub-sample \mathcal{X}_E is denoted as $\tilde{\eta}_{\hat{\tau},r}^E(\mathbf{s}_j)$.

To combine information from both data splits and across different FPCA directions, we define the detection statistic for each j as:

$$(12) \quad W_j = \sum_{r=1}^R \hat{\eta}_{\hat{\tau},r}^O(\mathbf{s}_j) \tilde{\eta}_{\hat{\tau},r}^E(\mathbf{s}_j).$$

This statistic fulfills the symmetry property under \mathcal{H}_0^j and tends to take large positive values under \mathcal{H}_1^j , as discussed further in Section 4.2. Based on the computed W_j values across all

locations, we determine a threshold $L > 0$ according to the following rule:

$$(13) \quad L = \inf \left\{ t > 0 : \frac{1 + \#\{j : W_j \leq -t\}}{\#\{j : W_j \geq t\} \vee 1} \leq \alpha \right\},$$

where α denotes the target FDR level. If the set is empty, we simply let $L = +\infty$. The desired support set is then recovered by $\mathcal{M} = \{j : W_j \geq L\}$.

To implement the multiple testing statistic in (12), a similar FVE criterion for the truncation number \widehat{R} can be employed as in the change-detection statistic Q_h . For bandwidth selection, we typically use a common h in $\widehat{\eta}_{\widehat{\tau},r}^E(\mathbf{s}_j)$ across all locations \mathbf{s}_j , following the same approach outlined in Algorithm 1. To ensure the theoretical guarantees for the kernel estimator in Assumption 4.5, a relatively large threshold value of ρ is determined for practical applicability. Remarkably, our method also accommodates varying h values at each \mathbf{s}_j to account for spatial inhomogeneity or differing clustering patterns, based on the researchers' knowledge of the local signal magnitude. We summarize the proposed functional SDA (fSDA) procedure as follows.

Algorithm 2 The fSDA procedure for support recovery

- 1: Obtain the estimated change-point $\widehat{\tau}$ as outlined by Algorithm 1.
- 2: Split the data into \mathcal{X}_O and \mathcal{X}_E as (10) and conduct the FPCA procedure on each split separately.
- 3: Determine the truncated number \widehat{R} using the same FVE criterion in Algorithm 1.
- 4: For each $j = 1, \dots, p$,
 - calculate $\widehat{\eta}_{\widehat{\tau},r}^O(\mathbf{s}_j)$ by (5) across $r = 1, \dots, \widehat{R}$ based on the FPCA estimates on \mathcal{X}_O .
 - calculate $\widehat{\eta}_{\widehat{\tau},r}^E(\mathbf{s}_j)$ by (11) across $r = 1, \dots, \widehat{R}$ based on the FPCA estimates on \mathcal{X}_E and the kernel function \mathbf{K}_h in Algorithm 1.
 - obtain the test statistic W_j by (12).
- 5: Rank W_j 's and obtain the threshold L by (B.5) for a target α . Finally, output the support set

$$\mathcal{M} = \{j : W_j \geq L\}.$$

4.2. *An intuitive explanation of the fSDA procedure.* As seen from the procedure in Section 4.1, the statistics W_j 's play a central role in the proposed fSDA approach. To explain why this works, let $T_{j,r}^O = \widehat{\eta}_{\widehat{\tau},r}^O(\mathbf{s}_j)$, which asymptotically follows $N(0, 1)$ under the null hypothesis, and let $T_{j,r}^E = \widehat{\eta}_{\widehat{\tau},r}^E(\mathbf{s}_j)$. For each r , the product $W_{j,r} = T_{j,r}^O T_{j,r}^E$ aggregates evidence from the two groups. When the signal magnitude at location \mathbf{s}_j , defined as $\Delta_{j,r} := \langle \Delta(\mathbf{s}_j; \cdot), \psi_r(\cdot) \rangle_{\mathcal{T}}$ is large, both $T_{j,r}^O$ and $T_{j,r}^E$ tend to exhibit large absolute values with the same sign. This results in a large positive $W_{j,r}$, and thus a large W_j , which aids in ranking and selecting informative locations. On the other hand, negative W_j 's, typically corresponding to the null cases, are useful for thresholding. Intuitively, W_j is, at least asymptotically symmetric with mean zero for $j \in \mathcal{A}^c$, due to the asymptotic normality of $T_{j,r}^O$ and the independence between \mathcal{X}_O and \mathcal{X}_E . The key idea is to leverage the following symmetry property:

$$(14) \quad \sup_{0 \leq t \leq c_p} \left| \frac{\sum_{j \in \mathcal{A}^c} \mathbb{I}(W_j \geq t)}{\sum_{j \in \mathcal{A}^c} \mathbb{I}(W_j \leq -t)} - 1 \right| = o_p(1)$$

for some upper bound c_p . Under the selection rule in (B.5), this implies that the number of false discoveries, $\#\{j \in \mathcal{A}^c : W_j \geq t\}$, is asymptotically equal to $\#\{j \in \mathcal{A}^c : W_j \leq -t\}$, which is conservatively approximated by $\#\{j : W_j \leq -t\}$. Therefore, the ratio in (B.5) provides an overestimate of FDP, leading to conservative control of FDR. Moreover, since most

elements in $\{j : W_j \leq -L\}$ are expected to belong to the null set for a suitably chosen L , the discrepancy between the fraction in (B.5) and the actual FDP is typically small in practice, ensuring that the empirical FDR level closely matches α . In summary, the proposed procedure approximates the FDP based on the symmetry of the ranking statistics W_j 's, rather than relying on asymptotic normality—which may be difficult to achieve due to the kernel aggregation approach.

Similar to the change-detection procedure in Algorithm 1, the proposed multiple testing approach can also be conducted based on a non-kernel version of W_j , computed directly from $\hat{\eta}_{\hat{\tau}, r}(\mathbf{s}_j)$ on both \mathcal{X}_O and \mathcal{X}_E . The corresponding ranking and thresholding process can be performed following the same steps as outlined in Algorithm 2, and we refer to this non-kernel variant as fSDA₀. Figure 1 illustrates a comparison between the operation of fSDA₀ and the kernel-based fSDA. The data are generated from the model (15) in Section 5 under scenario (i), where the spatial domain is a one-dimensional regular grid on $\mathcal{S} = [0, 1]$ with $p = 200$ locations. The alternative mean function is set as $\mu_1(\mathbf{s}, t) = 0.5 \mathbb{I}(\mathbf{s} \in \Omega_s)$ with $\Omega_s = [0.2, 0.8]$, resulting in a non-null set of size $|\mathcal{A}| = 120$. Panels (a) and (d) show scatterplots of W_j 's for fSDA₀ and fSDA, respectively, where black dots represent null locations and red triangles denote true signals. For both methods, the true signals predominantly appear above zero, while the uninformative W_j 's values (nulls) are roughly symmetrically distributed around the horizontal axis. This symmetry enables accurate estimation of the FDP, as defined by the fraction in (B.5) and illustrated in Panels (b) and (e), demonstrating the effectiveness of both methods in controlling FDR.

On the other hand, the proposed fSDA approach achieves a substantial improvement in power over fSDA₀. As shown in Figure 1, several true signals fall below the threshold in Panel (a), with some even falling below zero. In contrast, the kernel aggregation in (11) enables fSDA to effectively leverage spatial structure among neighboring locations, resulting in stronger positive values and observable clustering patterns among true signals, as illustrated in Panel (d). This refinement leads to a notable increase in TDP, as defined in (1), with Panel (f) showing consistently higher TDP values compared to Panel (c). Specifically, at an FDR level of 0.2, fSDA achieves a TDP of 0.98 with a threshold $L = 0.14$, significantly outperforming fSDA₀, which yields a TDP of 0.84 with $L = 0.30$. It is also noteworthy that, by utilizing an order-preserved strategy that harnesses the full sample information, both fSDA and fSDA₀ effectively mitigate the power loss commonly associated with conventional sample-splitting methods.

4.3. Theoretical property. In this section, we establish the asymptotic validity of the FDR control for the proposed fSDA procedure described in Algorithm 2. As is typical in multiple testing frameworks, we require that both n and p tend to infinity. Note that the test statistics W_j 's are constructed based on the estimated change-point $\hat{\tau}$, which remains consistent to τ^* as $p \rightarrow \infty$ according to Theorem 3.2. Specifically, we assume the following:

ASSUMPTION 4.1. (Order of location number to sample size) $p = o\{\exp(n^{1/4})\}$.

ASSUMPTION 4.2. (Moments) There exists $\gamma > 0$ such that $\mathbb{E}\{\exp(s \xi_{ir}(\mathbf{s}_j))\} \leq \exp(s^2 \gamma^2 \lambda_{r,j}/2)$ for all $j = 1, \dots, p$, $r = 1, \dots, R$ and $s \in \mathbb{R}$, i.e. the standardized FPC scores $\xi_{ir}(\mathbf{s}_j)/\lambda_{r,j}^{1/2}$ are sub-Gaussian random variables with variance proxy γ^2 . Furthermore, there exists a constant M independent of p such that $\sup_{j=1, \dots, p} \sum_{r=1}^{\infty} \lambda_{r,j} < M$.

Assumption 4.1 constrains the growth rate of p relative to n to facilitate technical derivations. Specifically, we apply the moderate deviation result for the two-sample t -statistic (Cao, 2007) to establish the uniform convergence of $\Pr(\eta_{j,r}^* > x)$ within $x \in (0, o(n^{1/6}))$, where

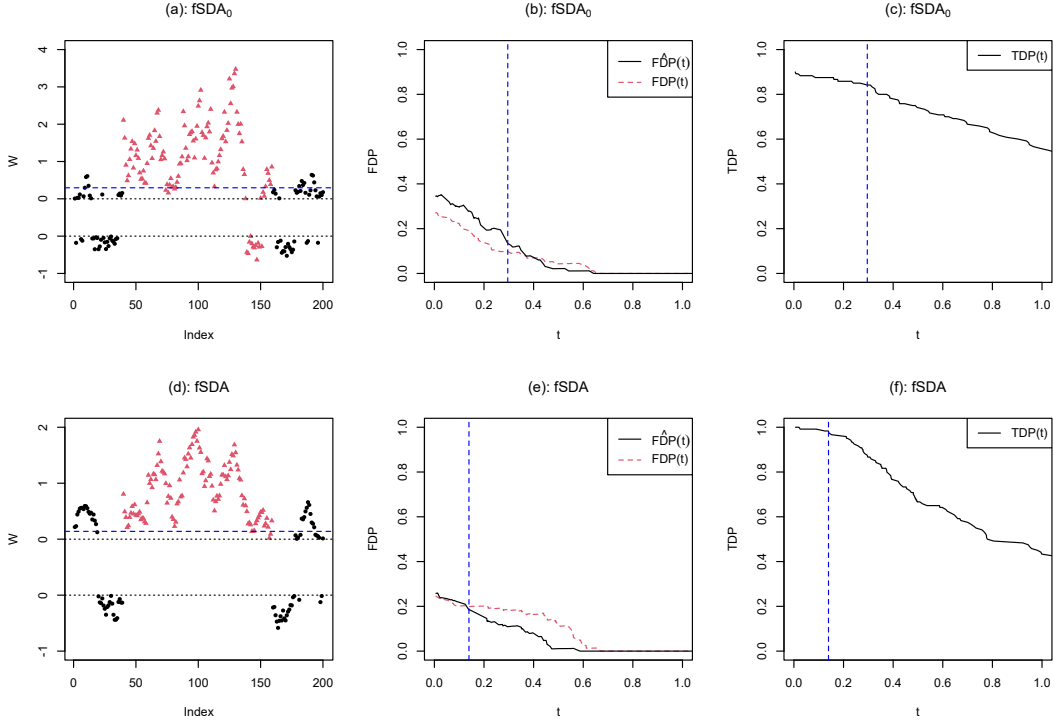


FIG 1. (a) Scatterplot of the 200 W_j 's obtained by $fSDA_0$ with black dots and red triangles denoting nulls and true signals, respectively. A vertical space is added to the middle of the plot to better contrast positive and negative W_j 's, and the blue dashed line represents the threshold L . (b) The corresponding estimate of FDP curve (against t) along with the true FDP for $fSDA_0$. (c) The TDP curve (against t) for $fSDA_0$. (d)-(f) The scatterplot, the corresponding FDP estimate, and the TDP for the $fSDA$ method.

$\eta_{j,r}^* := \lambda_{r,j}^{-1/2} \langle \widehat{\Delta}_{\tau^*}(\mathbf{s}_j; \cdot), \psi_r(\cdot) \rangle_{\mathcal{T}}$ denotes the oracle version of $\widehat{\eta}_{\hat{\tau},r}(\mathbf{s}_j)$ constructed using the true FPC elements. Assumption 4.2 is imposed to control the tail probability of $\eta_{j,r}^*$, and it additionally requires that the covariance function $C(\mathbf{s}_j, \cdot; \mathbf{s}_j, \cdot)$ be uniformly bounded in j . As shown in Zapata, Oh and Petersen (2022), this assumption ensures the derivation of concentration inequalities for estimators obtained via the FPCA approach. Moreover, we establish uniform bounds for the quantities $|\widehat{\lambda}_{r,j}^{-1/2} - \lambda_{r,j}^{-1/2}|$, $\|\widehat{\psi}_r(\cdot) - \psi_r(\cdot)\|_{\mathcal{T}}$, and $\langle \widehat{\Delta}_{\hat{\tau}}(\mathbf{s}_j; \cdot) - \widehat{\Delta}_{\tau^*}(\mathbf{s}_j; \cdot), \psi_r(\cdot) \rangle_{\mathcal{T}}$ in Lemma A.4, which provide more explicit concentration results than those in Theorem 2.1 and facilitate the derivation of the uniform convergence rate for W_j .

ASSUMPTION 4.3. (Signals) Define that $\boldsymbol{\delta}_j^* = (\delta_{j,1}^*, \dots, \delta_{j,R}^*)^T$ where $\delta_{j,r}^* = \lambda_{r,j}^{-1/2} \Delta_{j,r}$, and $\beta_p = \{1 \leq j \leq p : \sqrt{n} \|\boldsymbol{\delta}_j^*\| / \sqrt{\log p} \rightarrow \infty\}$. Assume that $b_p = |\beta_p| \rightarrow \infty$ as $n, p \rightarrow \infty$.

ASSUMPTION 4.4. (Dependence) For each $j = 1, \dots, p$, define that $\mathcal{C}_j = \{1 \leq k \leq p : \left| \sum_{r=1}^R \rho_r(\mathbf{s}_j, \mathbf{s}_k) \right| \geq C_\rho (\log n)^{-2-v}\}$, where $C_\rho > 0$ is a large constant, and $v > 0$ is some small constant. Assume that $|\mathcal{C}_j| \leq l_p$ for some l_p with $l_p/b_p \rightarrow 0$ as $n, p \rightarrow \infty$.

ASSUMPTION 4.5. (Bandwidth) For each j , the bandwidth h used in (11) satisfies that $\sup_{k: |k-j| \leq h} \sqrt{n} \|\boldsymbol{\delta}_k^* - \boldsymbol{\delta}_j^*\| = O(\sqrt{\log p})$.

Assumption 4.3 requires that the number of identifiable effect sizes, defined in terms of the standardized signal δ_j^* , does not become too small as $p \rightarrow \infty$. This is a standard requirement in FDP control methods. As demonstrated by Liu and Shao (2014), if a multiple testing approach controls the FDP with high probability, then the number of true alternatives must diverge as the number of tests goes to infinity. Assumption 4.4 allows $\xi_{ir}(\mathbf{s}_j)$ to be correlated across all locations, provided that the number of strong correlations does not grow too rapidly (Du et al., 2021). Since spatial correlation typically diminishes as the distance between locations increases, this assumption seems natural and can be satisfied if, for instance, the spatial random field is m -dependent (i.e. observations are independent if their distance exceeds m). Assumption 4.5 concerns the bandwidth condition for the proposed kernel aggregation approach. It is approximately satisfied when $nh^2 = O(\log p)$, given the smoothness of the mean function μ_i . From the perspective of estimation accuracy, this assumption ensures that $\tilde{\eta}_{\hat{\tau},r}(\mathbf{s}_j)$ serves as a reasonable approximation of $\hat{\eta}_{\hat{\tau},r}(\mathbf{s}_j)$, similarly to Assumption 2 in Du et al. (2021).

REMARK 2. We highlight that the obtained result for FDR control remains generally valid under various spatial sampling schemes, including both increasing and infill domain frameworks, as long as Assumptions 4.4–4.5 hold. As discussed in Cai, Sun and Xia (2022), an essential technical challenge in the context of the two-component mixture prior is to establish the uniform convergence of $\sum_{j=1}^p \mathbb{I}(p_j^w \leq t, \theta_j = 0) / \sum_{j=1}^p \pi(\mathbf{s}_j) t$, where p_j^w denotes the weighted p -value. Achieving this convergence relies on an accurate estimation of $\hat{\pi}(\cdot)$ under an infill-domain asymptotic regime. In contrast, our proposed fSDA procedure is independent of any p -value model; its validity primarily depends on the asymptotic symmetry property (14). This property can typically be satisfied under the dependence structure specified in Assumption 4.4, ensuring uniform convergence of $\sum_{j \in \mathcal{A}^c} \mathbb{I}(W_j \geq t) / \sum_{j \in \mathcal{A}^c} \mathbb{I}(W_j \leq -t)$, as shown in the proof of (33) in Appendix. Alternatively, one may impose other assumptions on the dependence structure, such as the mixing conditions on W_j 's or $\xi_{ir}(\cdot)$ (e.g. Yun and Bo, 2022), to achieve similar outcomes.

THEOREM 4.1. *Suppose the assumptions in Theorem 3.2 and Assumptions 4.1–4.5 hold, then for any $\alpha \in (0, 1)$, the FDP of the fSDA method satisfies*

$$\text{FDP}_w(L) := \frac{\#\{j : W_j \geq L, j \in \mathcal{A}^c\}}{\#\{j : W_j \geq L\} \vee 1} \leq \alpha + o_p(1).$$

It follows that $\limsup_{(n,p) \rightarrow \infty} \text{FDR}_w \leq \alpha$.

Theorem 4.1 confirms the asymptotic validity on FDR control of the proposed support recovery approach. In contrast to existing multiple testing methods, our fSDA procedure incorporates both kernel smoothing and sample-splitting, with test statistics constructed from FPCA estimators under a spatiotemporal change-point model. These components introduce additional challenges for both theoretical analysis and computational implementation. To better present the theoretical results in Theorem 4.1, we summarize the key uniform convergence results in Lemmas A.3–A.4 in Appendix A, which serve as the foundation for deriving the convergence rate of the ranking statistic W_j . The next result further demonstrates that our fSDA procedure is capable of not only maintaining FDR control, but also guaranteeing the full recovery of identifiable effect sizes.

COROLLARY 4.1. *Under the assumptions in Theorem 4.1, we have*

$$\limsup_{(n,p) \rightarrow \infty} \Pr(\mathcal{M} \supseteq \beta_p) = 1.$$

The detailed proofs of Theorem 4.1 and Corollary 4.1 are provided in Appendices B.5–B.6 of Appendix and the numerical performance of the proposed method is assessed through simulations in Section 5.

5. Monte Carlo simulation.

5.1. *Data generating process.* For $i = 1, \dots, n$, we generate the spatiotemporal data $X_i(\cdot; \cdot)$ as follows:

$$(15) \quad X_i(\mathbf{s}_j; t) = \mu_i(\mathbf{s}_j; t) + \sum_{r=1}^R \xi_{ir}(\mathbf{s}_j) \psi_r(t), \quad j = 1, \dots, p, \quad t \in \mathcal{T},$$

where $R = 6$ and the eigenfunctions are $\psi_r(t) = \sqrt{2} \cos\{r\pi t\}$ for odd r , and $\psi_r(t) = \sqrt{2} \sin\{(r-1)\pi t\}$ for even r . The time domain is set as $\mathcal{T} = [0, 1]$ with 100 equally spaced time points. The following three scenarios of the spatial domain are investigated, with the locations $\{\mathbf{s}_j\}_{j=1}^p$ being generated:

- (i) at a 1-dim regular grid $\{\frac{1}{p}, \frac{2}{p}, \dots, 1\}$ on $\mathcal{S} = [0, 1]$;
- (ii) at a 2-dim regular grid $\{\frac{1}{\sqrt{p}}, \frac{2}{\sqrt{p}}, \dots, 1\} \otimes \{\frac{1}{\sqrt{p}}, \frac{2}{\sqrt{p}}, \dots, 1\}$ on $\mathcal{S} = [0, 1] \times [0, 1]$;
- (iii) from a homogeneous Poisson process on $\mathcal{S} = [0, 1] \times [0, 1]$ with p (irregular) points.

For each i and $r = 1, \dots, R$, the FPC score $\xi_{ir}(\cdot)$ is generated from a mean-zero Gaussian random field with the covariance structure $\sigma_r(\mathbf{s}, \mathbf{s}') = \omega_r \mathbf{M}(\|\mathbf{s} - \mathbf{s}'\|; \nu_r, \phi_r)$, where $\omega_r = 4r^{-1.6}$ and $\mathbf{M}(\cdot; \nu, \phi)$ denote the isotropic Matérn covariance with the smoothing parameter ν and range parameter ϕ . Following Liang et al. (2023) and to reflect the magnitude of weak separability, we set $\nu_1 = 1$ and $\nu_r = 0.5$ for $r = 2, \dots, 6$, whereas $(\phi_1, \phi_2, \phi_3, \phi_4) = (0.1, 0.05, 0.075, 0.02)$ and $\phi_5 = \phi_6 = 0$, i.e. no spatial correlation for the high-order FPC scores. The true change-point is set as $\tau^* = n/2$. We define the mean function before the change-point as $\mu_i(\mathbf{s}; t) = \mu_0(\mathbf{s}; t) = 0$ for $1 \leq i \leq \tau^*$, and the alternative mean as

$$(16) \quad \mu_i(\mathbf{s}; t) = \mu_1(\mathbf{s}; t) = \delta K_\Omega(\|\mathbf{s} - \mathbf{s}_0\|), \quad \text{for } i = \tau^* + 1, \dots, n,$$

where $K_\Omega(\cdot)$ is a univariate Gaussian kernel function with the support $\Omega = \{\mathbf{s} \in \mathcal{S} : \|\mathbf{s} - \mathbf{s}_0\| \leq r_s\}$ and \mathbf{s}_0 being the center of \mathcal{S} . According to the definition in (16), the parameters δ and r_s reflect the strength and magnitude of the spatial signal, respectively. We first implement the global change-point detection outlined in Algorithm 1. For the alternative case with $\delta > 0$, the support recovery procedure is then performed following Algorithm 2.

For space considerations, we only present the test results under scenario (iii), i.e. the irregular 2-dimensional case, which most closely resembles the structure of China's precipitation data analyzed in Section 6 and is more representative of practical applications. Our simulations also show satisfactory results for the other two scenarios, demonstrating the robustness of our method across different spatial sampling schemes. We also investigate the impact of spatial covariance on the test performance by varying the range parameters, with more simulation results provided in Appendix E.1.

5.2. *Results for change-point detection.* We implement the proposed change-point detection approach using either the “max” or “sum” statistic of Q_h and Q_0 . The truncation number R and bandwidth h are determined based on the procedure outlined in Section 3.2. The test results are shown to be robust across FVE values in the range $[0.8, 0.95]$ and ϱ values in $[0.01, 0.1]$, with the latter yielding an average h value in $[0.18, 0.47]$. For clarity and brevity, we present the results under FVE= 90% and $\varrho = 0.05$. We compare the performance of our

TABLE 1
Empirical size (%) of the change-point tests under different (p, n) -settings.

Method	Type	$n = 100$			$n = 200$		
		$p = 20$	$p = 50$	$p = 100$	$p = 20$	$p = 50$	$p = 100$
Q_0	sum	5.0	5.4	4.5	5.5	5.6	4.5
	max	4.5	3.4	4.4	5.2	4.3	4.0
Q_h	sum	5.2	5.8	5.5	5.6	5.3	5.0
	max	6.0	6.3	6.2	5.5	5.7	5.6
Gro	$\hat{\Lambda}_1$	7.2	6.9	5.7	6.9	6.7	5.5
	$\hat{\Lambda}_2$	7.8	10.1	9.8	7.9	9.1	8.1

methods with the statistics $\hat{\Lambda}_1$ and $\hat{\Lambda}_2$ from Gromenko, Kokoszka and Reimherr (2017) (referred to as Gro) under the same FVE criterion. Here, $\hat{\Lambda}_1$ can be considered as a counterpart to Q_0^{sum} under the assumption of strong separability, while $\hat{\Lambda}_2$ is a non-normalized version of $\hat{\Lambda}_1$. The empirical size and power are assessed through 1000 and 200 runs respectively, conducted at a 0.05 significant level.

Table 1 compares the empirical Type I errors using the proposed statistics with those using $\hat{\Lambda}_1$ and $\hat{\Lambda}_2$ across various sample sizes and numbers of locations. The proposed tests using Q_0 and Q_h exhibit overall stable sizes for both “sum” and “max” types across different values of p and n . In contrast, the test using $\hat{\Lambda}_2$ fails to control the Type I errors, while the test using $\hat{\Lambda}_1$ appears to be oversized when p is relatively small. For the proposed kernel statistic Q_h , the empirical sizes tend to be closer to the nominal level as the sample size n increases from 100 to 200, with little difference observed between the “sum” and “max” statistics.

Table 2 presents the empirical power results for $n = 100$ under various scenarios of spatial signals, with the highest power in each scenario highlighted in bold. The results for $n = 200$, which show a clear improvement in power, are deferred to the Appendix E.1 due to space constraints. It can be seen that the test using Q_h , whether employing the “sum” or “max” statistic, generally outperforms other methods across different settings. As the spatial magnitude r_s increases from 0.4 to 0.6, the proportion of locations with mean changes rises significantly, from 48.8% to 94.6%, resulting in a rapid increase in the power of Q_h . In contrast, the power of Q_0 and $\hat{\Lambda}_1$ remains relatively unchanged, indicating the superiority of Q_h as the signal magnitude grows. Additionally, all methods exhibit improved performance as p increases, with Q_h demonstrating the most significant enhancement in power. This aligns with the intuition that denser locations allow kernel aggregation to integrate more information from the neighborhood, underscoring the advantages of incorporating spatial clustering patterns into inference.

We further assess the performance of the proposed change-point estimation approach in terms of the mean and standard deviation. As shown in Table 3, the change detection using Q_h exhibits the smallest estimation errors across nearly all settings, particularly for smaller δ and larger p . When the signal strength δ increases to 1, all methods except $\hat{\Lambda}_2$ achieve 100% power with significantly improved accuracy in change-point estimation, and Q_h continues to demonstrate greater efficiency than Q_0 and $\hat{\Lambda}_1$. The additional result with $r_s = 0.6$, provided in Appendix E.1, also illustrate the superior consistency of Q_h compared to the other methods for larger signal magnitudes.

5.3. *Results for support recovery.* After estimating the change point for each simulated dataset under the alternatives, we assess the performance of support recovery using the following methods: (i) BH procedure, (ii) LAWS procedure, (iii) the fSDA₀ procedure without kernel aggregation, and (iv) The full fSDA procedure. Both the BH and LAWS methods

TABLE 2
Empirical power (%) of the change-point tests under different signal settings when $n = 100$.

	Method	Type	$r_s = 0.4$			$r_s = 0.6$		
			$\delta = 0.2$	$\delta = 0.3$	$\delta = 0.4$	$\delta = 0.2$	$\delta = 0.3$	$\delta = 0.4$
$p = 20$	Q_0	sum	19.0	31.5	49.0	16.0	33.0	53.5
		max	12.5	30.5	46.5	14.0	28.0	52.0
	Q_h	sum	20.0	35.5	53.5	25.0	45.0	67.0
		max	20.0	38.5	51.5	23.5	46.5	65.0
	Gro	$\widehat{\Lambda}_1$	19.0	28.5	46.5	17.0	27.5	48.0
		$\widehat{\Lambda}_2$	9.0	11.0	20.0	10.0	11.0	27.0
$p = 50$	Q_0	sum	23.0	47.0	68.5	17.0	42.5	69.5
		max	14.5	40.0	65.0	9.5	44.0	68.5
	Q_h	sum	31.5	59.5	78.0	30.0	73.0	84.0
		max	30.0	57.5	77.5	28.0	75.0	86.0
	Gro	$\widehat{\Lambda}_1$	20.5	44.0	65.5	17.5	39.5	68.0
		$\widehat{\Lambda}_2$	17.0	30.0	32.0	12.0	28.0	34.5
$p = 100$	Q_0	sum	24.5	51.5	79.5	15.5	52.5	82.5
		max	14.0	48.5	80.0	10.5	49.0	81.0
	Q_h	sum	36.0	76.0	91.5	44.5	88.0	98.5
		max	30.0	71.0	92.0	37.5	89.5	98.0
	Gro	$\widehat{\Lambda}_1$	22.5	47.5	78.0	19.5	54.5	80.5
		$\widehat{\Lambda}_2$	19.5	31.5	42.0	17.5	26.5	45.0

TABLE 3
Simulation study on the consistency of the change-point detection procedures with the mean and standard deviation (in parentheses) of $|\hat{\tau} - \tau^*|$'s with $r_s = 0.4$ and $n = 100$.

Method	$\delta = 0.4$			$\delta = 1$		
	$p = 20$	$p = 50$	$p = 100$	$p = 20$	$p = 50$	$p = 100$
Q_0	3.48(3.62)	2.52(3.08)	2.38(2.63)	0.72(1.28)	0.52(1.05)	0.22(0.60)
Q_h	3.55(3.73)	2.43(2.76)	1.95(2.54)	0.72(1.24)	0.50(1.01)	0.21(0.54)
$\widehat{\Lambda}_1$	4.12(3.88)	2.76(3.21)	2.58(2.69)	0.74(1.34)	0.59(1.08)	0.24(0.60)
$\widehat{\Lambda}_2$	5.22(4.67)	4.92(4.56)	4.31(4.48)	1.83(2.53)	1.53(2.30)	0.81(1.17)

employ a p -value screening approach based on the asymptotic normality of $\hat{\eta}_{\hat{\tau}, r}(\mathbf{s}_j)$ from (5). For LAWS, a nonparametric estimator for the prior probability $\pi(\mathbf{s}_j)$ is employed with the bandwidth selected by the R-package “kedd”. In our fSDA method, the truncation number R and bandwidth h are determined according to Algorithm 2. Under a nominal level at $\alpha = 0.2$, these methods are compared based on empirical FDR and average power, defined as $\text{AP} = \mathbb{E}(\text{TDP})$, across 200 replications. Figure 2 illustrates the multiple testing results for $p = 50, 100$, and 200 with $n = 100$. Additional results with $n = 200$ are provided in Appendix E.1, showing a similar FDR pattern along with increased power.

From Figure 2, it is evident that all methods, except LAWS, control the FDR at the nominal level in most settings, with BH being more conservative due to overestimating false positives. The FDR for all methods tends to decrease as the spatial magnitude r_s increases, whereas LAWS exhibits substantial FDR inflation when $r_s = 0.3$ and 0.4. When $r_s = 0.5$, corresponding to an 80% proportion of the informative set, even LAWS is able to control the FDR. It is also noteworthy that inflated FDR levels are observed for both BH and LAWS when the values of r_s and δ are relatively small. This deficiency may stem from inaccurate

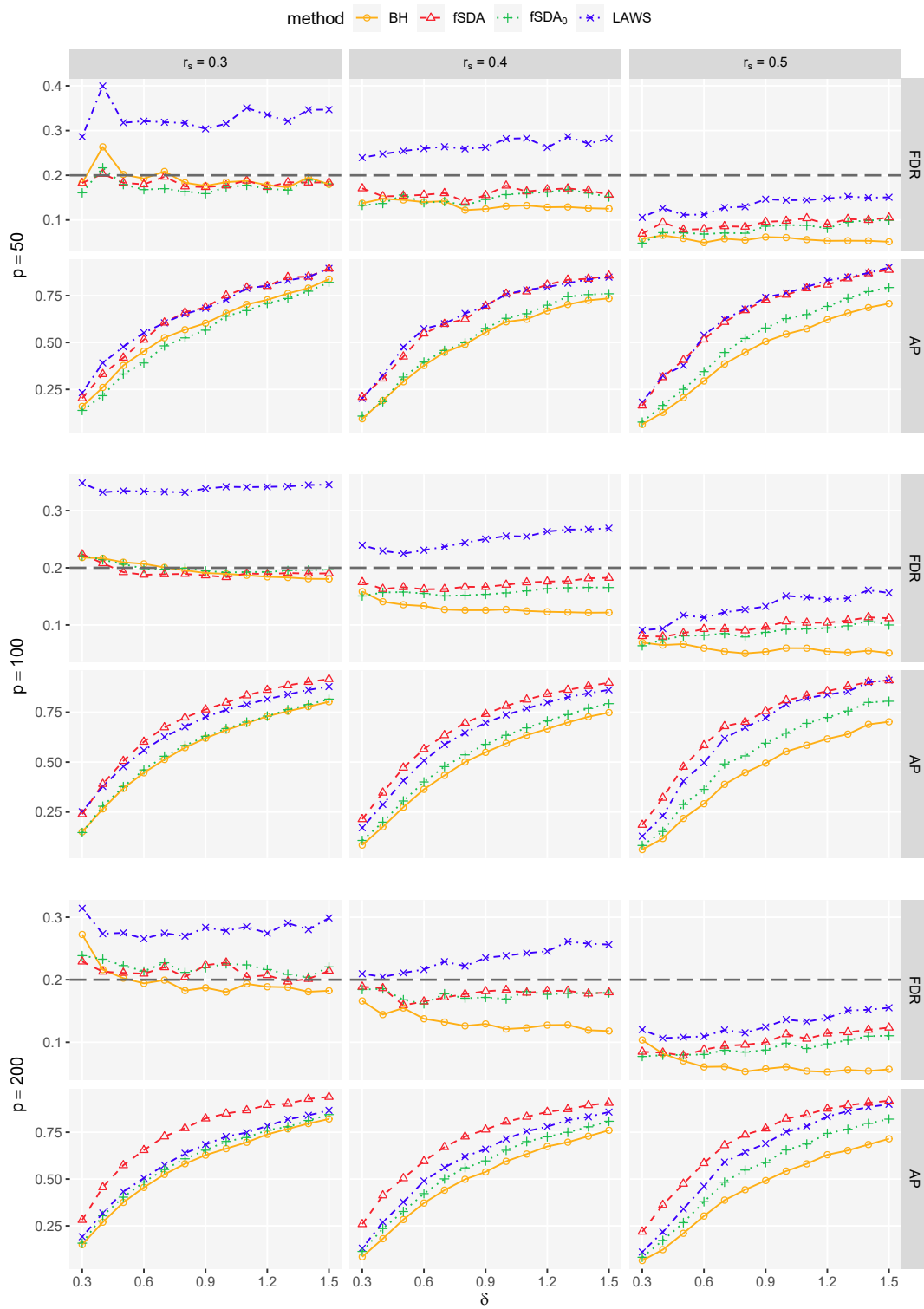


FIG 2. The empirical FDR and AP comparison for $n = 100$, with the dashed line representing the nominal level $\alpha = 0.2$.

estimation of the p -values when signals are weak, further demonstrating the advantage of the proposed p -value-free approach.

In terms of average power, the fSDA method consistently outperforms the other approaches across different r_s and δ , with its superiority becoming more pronounced as p increases. Even for $p = 50$, the power of fSDA remains comparable to LAWS, which fails to control the FDR when r_s is less than 0.4. While fSDA₀ also controls the empirical FDR across various scenarios, its power is notably inferior to those of fSDA. These findings are similar to those from in Table 2, demonstrating that the kernel statistic effectively aggregates spatial signals, particularly when stations are more densely located. Additionally, all methods exhibit higher power as the signal strength δ increases, though varying the magnitude r_s has a less noticeable impact on power. In conclusion, the proposed fSDA method offers the most powerful approach while maintaining effective FDR control, and the results demonstrate robustness across different values of n and p .

6. Empirical application to China’s precipitation data. The study of precipitation plays an important role in the fields of climatology, meteorology, and hydrology (e.g. Brunsell, 2010; Liu et al., 2019). Precipitation data in China, influenced by Asian monsoon and complex terrain, exhibit intricate spatial and temporal patterns with notable seasonal, inter-annual, and regional variations (Ng, Zhang and Li, 2021; Zhang, Zhu and Yin, 2019). The data analyzed in this study were provided by the National Meteorological Information Center, China Meteorological Administration (CMA), consisting of daily precipitation records from over 1500 meteorological stations across mainland China from 1961 to 2013. Following standard environmental practices, we aggregate the daily observations into half-month intervals, resulting in $12 \times 2 = 24$ records per year. Due to the vast and complex landscape in China, we select a subset of $p = 100$ meteorological stations in Eastern China for this analysis. Panel (a) of Figure 3 visualizes the geographical locations of the selected subregion, including the provinces of Shandong, Jiangsu, Anhui, Shanghai, Zhejiang, Jiangxi, and Fujian, which comprise one of the areas with the highest precipitation levels in China.

To mitigate the impact of heavy-tailed distributions, we apply a logarithmic transformation to the original half-monthly precipitation data $Y_i(\mathbf{s}_j; t_m)$ for year i at time point t_m , $m = 1, \dots, 24$:

$$X_i(\mathbf{s}_j; t_m) = \log_{10}\{Y_i(\mathbf{s}_j; t_m) + 1\},$$

as recommended by Gromenko, Kokozska and Reimherr (2017). The transformed temporal records at each location are then projected onto the functional time domain $\mathcal{T} = [0, 1]$ using cubic smoothing splines with six degrees of freedom. Based on the resulting pre-smoothed spatially index functional dataset $\{X_i(\mathbf{s}_j; t) : i = 1961, \dots, 2013; j = 1, \dots, p; t \in \mathcal{T}\}$, our objective is to apply the proposed methodology to detect a potential change-point year and subsequently identify the specific spatial locations where significant mean changes occur.

Before proceeding with the change-detection procedure, it is crucial to evaluate the space-time separability structure of the dataset. Additional results in Appendix E.2 demonstrate that the hypothesis of strong separability is rejected for our data, whereas the assumption of weak separability is not rejected across different FVE levels. Given the validity of the weakly separable model, we first apply the proposed FPCA procedure outlined in Algorithm 1. At a 90% level of FVE, the selected number of eigenfunctions is $\widehat{R} = 5$. Using the bandwidth selection rule, we set $h = 487.1\text{km}$, slightly larger than the mean (351.7km) and the median (323.8km) of the pairwise distances among all spatial locations. It is also noteworthy that the change-detection procedure yields similar results over a reasonable range, specifically with $4 \leq \widehat{R} \leq 8$ and $300\text{km} \leq h \leq 700\text{km}$.

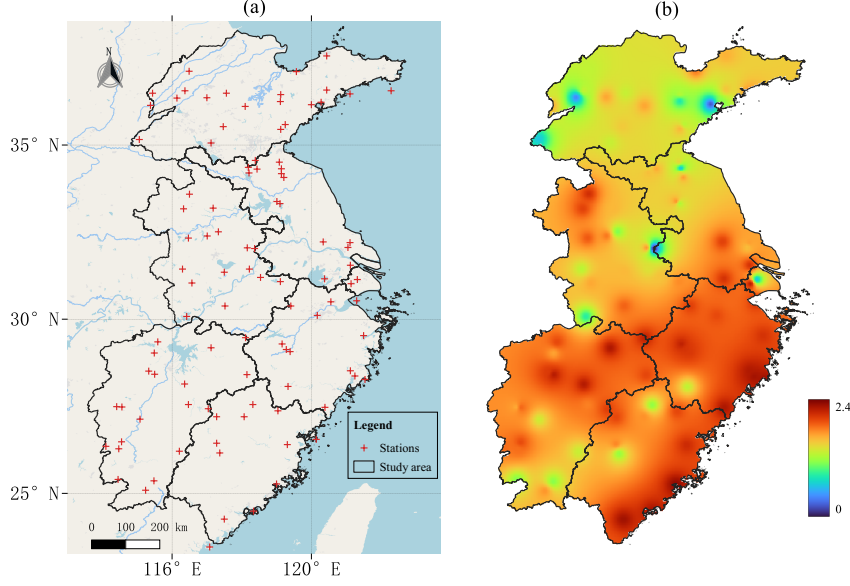


FIG 3. (a) Illustration of 100 meteorological stations in Eastern China. (b) A heatmap of the estimated spatial field of $\|\hat{\mu}_0(\mathbf{s}; \cdot) - \hat{\mu}_1(\mathbf{s}; \cdot)\|_{\mathcal{T}}$ before and after 1988.

TABLE 4

The p -values of change-point tests for China precipitation data.

Gro		Q_0		Q_h	
$\hat{\Lambda}_1$	$\hat{\Lambda}_2$	sum	max	sum	max
0.370	0.385	0.035	0.005	0.025	< 0.001

TABLE 5

The p -values of change-point test for different segment of years.

Segment	Gro		Q_0		Q_h	
	$\hat{\Lambda}_1$	$\hat{\Lambda}_2$	sum	max	sum	max
1961-1988	0.915	0.885	0.495	0.675	0.890	0.945
1989-2013	0.715	0.755	0.520	0.665	0.665	0.750

We perform the change-point test using both “max” and “sum” types of Q_h , as well as Q_0 . As shown in Table 4, all tests using Q_h and Q_0 reject the null hypothesis, with Q_h yielding slightly smaller p -values compared to Q_0 . In contrast, the statistics $\hat{\Lambda}_1$ and $\hat{\Lambda}_2$ from Gromenko, Kokoszka and Reimherr (2017) fail to detect a change-point. We then plot the function $Q_h(\tau)$ in Figure 7 of Appendix E.2 which identifies the estimated change-year as $\hat{\tau} = 1988$. This finding is consistent with the results of Liu et al. (2019), which indicated that change-points in precipitation extremes increasingly occurred around 1990 in the southeastern region of the Hu Huanyong line, a vast and well-known area fully encompassing our selected locations. Further tests conducted separately on the two segmented periods, as summarized in Table 5, confirm that no additional change-points are present apart from the year 1988.

To figure out the locations that contributed to the changes in $\hat{\tau} = 1988$, we begin by exploring the spatial distribution of the mean difference. Specifically, an ordinary kriging interpola-

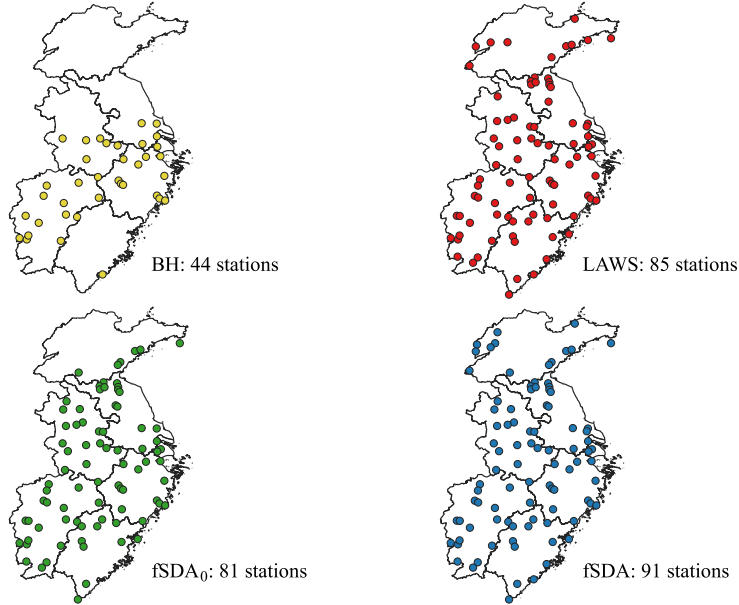


FIG 4. The recovery sets of meteorological stations using various multiple testing approaches.

tion approach is applied to the quantity $\|\hat{\mu}_0(\mathbf{s}; \cdot) - \hat{\mu}_1(\mathbf{s}; \cdot)\|_{\mathcal{T}}$ with an exponential variogram, where

$$(17) \quad \hat{\mu}_0(\mathbf{s}; t) = \hat{\tau}^{-1} \sum_{i=1}^{\hat{\tau}} X_i(\mathbf{s}; t) \text{ and } \hat{\mu}_1(\mathbf{s}; t) = (n - \hat{\tau})^{-1} \sum_{i=\hat{\tau}+1}^n X_i(\mathbf{s}; t)$$

represent the estimated mean functions for the periods before and after the detected change-point, respectively. As indicated in Panel (b) of Figure 3, aside from a few areas where the kriging estimates of this mean-difference is nearly zero, most of Eastern China experienced notable changes in the amount of precipitation, with a more pronounced increasing trend in the southern part of the selected region. While this method provides a rough and intuitive sketch of the spatial patterns, it falls short of rigorously identifying the specific subsets of locations where significant changes have occurred.

To accurately identify the regions contributing to the observed changes, we perform the multiple testing procedure as outlined in (P2) across these 100 stations. Using an FDR level of $\alpha = 0.2$, we implement the proposed fSDA approach following Algorithm 2 and compare it with the BH, LAWS, and fSDA₀ methods. As shown in the detection results in Figure 4, fSDA recovers the largest set of contributing stations, while BH identifies the fewest. All methods highlight a majority of stations in Zhejiang, Jiangxi, and the southern part of Anhui and Jiangsu, areas that display the most substantial differences in precipitation, as shown in Figure 3(b). In comparison to BH, the other three methods identify additional stations in Fujian, a highly informative area in the heatmap of Figure 3(b). Both fSDA₀ and fSDA detect over 80 stations, with fSDA capturing more stations located contiguously in northwest Shandong. The result from LAWS, which detects 85 stations, shows some disparity compared to fSDA, particularly in Shandong and northern Anhui. Given the superior FDR control of fSDA as demonstrated by our simulation study, we recommend its discovery set as a more accurate identification of the changing regions. Our detection results align with the notable north-south disparity around the Yangtze River observed by Liu et al. (2019) and pinpoint specific locations exhibiting significantly increasing trends. However, further research, in-

cluding a more detailed environmental analysis of the specific precipitation changes at each location, is necessary to deepen our understanding of these findings.

APPENDIX A: MAIN LEMMAS

In this section, we provide several key lemmas that characterize the convergence properties of the proposed detection statistics and serve as fundamental components in the proof of the main theorems. We begin with a weak convergence result for the i.i.d. sum of FPC scores.

LEMMA A.1. *Suppose that Assumptions 2.1–2.4 hold. Then the FPC scores $\{\xi_{ir}(\mathbf{s}_j) : i = 1, \dots, n; r = 1, \dots, R; j = 1, \dots, p\}$ satisfy the functional central limit theorem (with respect to the Skorokhod space $D^{pR}[0, 1]$) that*

$$(18) \quad n^{-1/2} \sum_{1 \leq i \leq nx} \text{vec} \begin{pmatrix} \xi_{i1}(\mathbf{s}_1) & \dots & \xi_{iR}(\mathbf{s}_1) \\ \vdots & \ddots & \vdots \\ \xi_{i1}(\mathbf{s}_p) & \dots & \xi_{iR}(\mathbf{s}_p) \end{pmatrix} \xrightarrow{d} \mathbf{W}(x)$$

for $x \in (0, 1)$, where $\mathbf{W}(x)$ is a pR -dimensional vector of Brownian motions with block-diagonal covariance matrix $\Sigma = \text{diag}(\Sigma_1, \dots, \Sigma_R)$.

Define that $\boldsymbol{\eta}_j^* = (\eta_{j,1}^*, \dots, \eta_{j,R}^*)^\top$ where $\eta_{j,r}^* = \lambda_{r,j}^{-1/2} \left\langle \widehat{\Delta}_{\tau^*}(\mathbf{s}_j; \cdot), \psi_r(\cdot) \right\rangle_{\mathcal{T}}$ denotes the counterpart of $\hat{\eta}_{j,r} := \hat{\eta}_{\hat{\tau},r}(\mathbf{s}_j)$ using the true FPC scores. Define similarly that $\tilde{\boldsymbol{\eta}}_j^* = (\tilde{\eta}_{j,1}^*, \dots, \tilde{\eta}_{j,R}^*)^\top$ where $\tilde{\eta}_{j,r}^* = \sum_k K_h(\mathbf{s}_k - \mathbf{s}_j) \eta_{k,r}^* / \sum_k K_h(\mathbf{s}_k - \mathbf{s}_j)$. The next lemma describes the moment and uniform bounds for $\boldsymbol{\eta}_j^*$ and $\tilde{\boldsymbol{\eta}}_j^*$.

LEMMA A.2. *Suppose that the process $\mathbf{X}_i(\cdot)$ is weakly separable under Assumption 2.4. (a) The covariance matrix of $\boldsymbol{\eta}_j^*$, denoted as Σ_j^* , is diagonal with the entries equal to $\theta_0(1 - \theta_0)(1 - 2\theta_0)$, where we assume $\theta_0 < 1/2$ without loss of generality. (b) Suppose Assumption 4.2 hold. Then for each $1 \leq j \leq p$,*

$$\Pr \left(\left\| \boldsymbol{\eta}_j^* - \sqrt{n} \theta_0 (1 - \theta_0) \boldsymbol{\delta}_j^* \right\| > \sqrt{C_\eta \log p} \right) = o(1/p)$$

for some large $C_\eta > 0$, and the same argument holds for $\tilde{\boldsymbol{\eta}}_j^*$ under Assumption 4.5.

Define $W_j^* := \sum_{r=1}^R \eta_{j,r}^{*O} \tilde{\eta}_{j,r}^{*E}$, which denotes the counterpart of the statistic (12) based on $\eta_{j,r}^*$ and $\tilde{\eta}_{j,r}^*$. Lemma A.3 provides the asymptotic symmetry property of W_j^* .

LEMMA A.3. *Suppose Assumptions 2.4, 4.1–4.2 and 4.4–4.5 hold. Then we have*

$$(19) \quad \sup_{0 \leq t \leq t^*} \left| \frac{\sum_{j \in \mathcal{A}^c} \mathbb{I}(W_j^* \geq t)}{\sum_{j \in \mathcal{A}^c} \mathbb{I}(W_j^* \leq -t)} - 1 \right| = o_p(1),$$

for some upper bound t^* with $t^* \leq C_\eta \log p$.

Lemma A.4 establishes the uniform bounds for the estimators used in W_j .

LEMMA A.4. *Suppose that $\mathbf{X}_i(\cdot)$ is weakly separable under Assumptions 2.1–2.4 and Assumption 4.2.*

(a) For each $1 \leq r \leq R$, we have

$$\max_{1 \leq j \leq p} \left| \hat{\lambda}_{r,j}^{-1/2} - \lambda_{r,j}^{-1/2} \right| = O_p \left((\log p/n)^{1/2} \right).$$

(b) For each $r = 1, \dots, R$, we have

$$\max_{1 \leq j \leq p} \left| \left\langle \widehat{\Delta}_{\hat{\tau}}(\mathbf{s}_j) - \widehat{\Delta}_{\tau^*}(\mathbf{s}_j), \psi_r \right\rangle_{\mathcal{T}} \right| = O_p \left((\log p/n)^{1/2} \right).$$

(c) Define that $\mathcal{A}_h^c = \mathcal{A}^c \cup \{k : |k - j| \leq h \text{ where } j \in \mathcal{A}^c\}$ and suppose Assumption 4.5 holds. Then for each $r = 1, \dots, R$,

$$\max_{j \in \mathcal{A}_h^c} |\hat{\eta}_{j,r} - \eta_{j,r}^*| = O_p \left(\log p/n^{1/2} \right).$$

(d) Under Assumption 4.1, we have

$$\max_{j \in \mathcal{A}^c} |W_j - W_j^*| = o_p \left((\log p)^{-1/2} \right)$$

APPENDIX B: TECHNICAL DETAILS

B.1. Proof of Theorem 2.1. We begin by introducing some standard definitions for the covariance operators in Hilbert spaces. Let $\mathcal{B}_{HS}\{L^2(\mathcal{T})\}$ denote the space of Hilbert-Schmidt operators on $L^2(\mathcal{T})$, which is itself a Hilbert space with the inner product $\langle \mathcal{C}_1, \mathcal{C}_2 \rangle_{HS} = \sum_{r=1}^{\infty} \langle \mathcal{C}_1 e_r, \mathcal{C}_2 e_r \rangle$ for any orthonormal basis $\{e_r\}$ in $L^2(\mathcal{T})$, and the induced norm $\|\cdot\|_{HS}$. For any $f_1, f_2 \in L^2(\mathcal{T})$, $f_1 \otimes f_2$ denotes the operator in $\mathcal{B}_{HS}\{L^2(\mathcal{T})\}$ defined by $(f_1 \otimes f_2)(g) = \langle f_1, g \rangle f_2$ for any $g \in L^2(\mathcal{T})$. Let $(L^2(\mathcal{T}))^p$ denote the space of p -dim functions with inner product $\langle \mathbf{f}, \mathbf{g} \rangle_{L^p} = \sum_{j=1}^p \int_{\mathcal{T}} f_j(t) g_j(t) dt$ for $\mathbf{f}, \mathbf{g} \in (L^2(\mathcal{T}))^p$, and the norm $\|\cdot\|_{L^p} = \langle \cdot, \cdot \rangle_{L^p}^{1/2}$. Recall that $\boldsymbol{\varepsilon}_i = \{\varepsilon_i(\mathbf{s}_1), \dots, \varepsilon_i(\mathbf{s}_p)\}^T$ is a p -dim mean-zero functional process in $(L^2(\mathcal{T}))^p$, where $\varepsilon_i(\mathbf{s}_j, \cdot)$ is abbreviated as $\varepsilon_i(\mathbf{s}_j)$ for the objective in $L^2(\mathcal{T})$. Define $\mathcal{C}_{jk} = \mathbb{E}\{\varepsilon_i(\mathbf{s}_j) \otimes \varepsilon_i(\mathbf{s}_k)\}$ for any $j, k = 1, \dots, p$, which is the covariance operator for $\varepsilon_i(\mathbf{s}_j)$ and $\varepsilon_i(\mathbf{s}_k)$ in $\mathcal{B}_{HS}\{L^2(\mathcal{T})\}$. Consequently, the covariance function $C(s_j, t; s_k, t')$, as defined in Section 2.1, can be regarded as the covariance kernel of the operator \mathcal{C}_{jk} . Moreover, the marginal covariance function $H(t, t')$ can be seen as the kernel of the marginal covariance operator defined by

$$\mathcal{H} = p^{-1} \sum_{j=1}^p \mathcal{C}_{jj}.$$

We refer to Chapters 7.2 and 7.3 of [Hsing and Eubank \(2015\)](#) for more details on the (cross) covariance operators in Hilbert space.

When the p -dim functional process $\boldsymbol{\varepsilon}_i$ is weakly separable, as defined in (2), the covariance operator of \mathcal{C}_{jj} entails the eigen-decomposition $\mathcal{C}_{jk} = \sum_{r=1}^{\infty} \sigma_r(\mathbf{s}_j, \mathbf{s}_k) \psi_r \otimes \psi_r$, which implies that

$$\mathcal{H} = \sum_{r=1}^{\infty} \lambda_r \varphi_r \otimes \varphi_r,$$

where $\{\lambda_r\}_{r=1}^R$ are the eigenvalues of the covariance function $H(t, t')$. Let $\widehat{\mathcal{H}}$ denote the operator corresponding to the empirical covariance $\widehat{H}(t, t')$ defined in (3). The key issue in proving Theorem 2.1 is to establish the uniform convergence rate of $\|\widehat{\mathcal{H}} - \mathcal{H}\|_{HS}$, as provided in (20). It can be shown that

$$\widehat{H}(t, t') - H(t, t') = \Gamma_1 + \Gamma_2,$$

where

$$\begin{aligned}\Gamma_1 &:= \frac{1}{p(n-1)} \left\{ \sum_{i=2}^{n-1} \langle \boldsymbol{\varepsilon}_i(t), \boldsymbol{\varepsilon}_i(t') \rangle_p \right\} - \frac{1}{p} \mathbb{E} \left\{ \langle \boldsymbol{\varepsilon}_i(t), \boldsymbol{\varepsilon}_i(t') \rangle_p \right\}, \\ \Gamma_2 &:= \frac{1}{2p(n-1)} \left\{ \langle \boldsymbol{\varepsilon}_1(t), \boldsymbol{\varepsilon}_1(t') \rangle_p + \langle \boldsymbol{\varepsilon}_n(t), \boldsymbol{\varepsilon}_n(t') \rangle_p \right. \\ &\quad \left. + \langle \boldsymbol{\Delta}(t), \boldsymbol{\Delta}(t') \rangle_p + 2 \langle \boldsymbol{\Delta}(t), \boldsymbol{\varepsilon}_{\tau^*+1}(t') - \boldsymbol{\varepsilon}_{\tau^*}(t') \rangle_p \right\},\end{aligned}$$

and $\boldsymbol{\Delta} = \{\Delta(\mathbf{s}_1), \dots, \Delta(\mathbf{s}_p)\}^T \in (L^2(\mathcal{T}))^p$. Denote $\widehat{C}_{jk} = (n-1)^{-1} \sum_{i=2}^n \varepsilon_i(\mathbf{s}_j) \otimes \varepsilon_i(\mathbf{s}_k)$ for any $j, k = 1, \dots, p$. It follows from Assumption 1 and Theorem 8.1.2 of [Hsing and Eubank \(2015\)](#) that $\widehat{C}_{jk} - C_{jk}$ converges weakly to a mean-zero Gaussian random element in $\mathcal{B}_{HS}\{L^2(\mathcal{T})\}$, which implies that $\widetilde{\Delta}_{jk} := \widehat{C}_{jk} - C_{jk} = O_p(n^{-1/2})$. By definition we further set $\Gamma_1 = p^{-1} \sum_{j=1}^p (\widehat{C}_{jj} - C_{jj})$, and it follows that

$$\mathbb{E} \|\Gamma_1\|_{HS}^2 \leq \frac{1}{p^2} \sum_{j=1}^p \mathbb{E} \|\widetilde{\Delta}_{jj}\|_{HS}^2 + \frac{1}{p^2} \sum_{j \neq k} \mathbb{E} \|\widetilde{\Delta}_{jj} \widetilde{\Delta}_{kk}\|_{HS}.$$

The first term on the right hand is $O((pn)^{-1})$ since $\mathbb{E} \|\widetilde{\Delta}_{jj}\|_{HS}^2 = O(n^{-1})$. For the second term, we have $\mathbb{E} \|\widetilde{\Delta}_{jj} \widetilde{\Delta}_{kk}\|_{HS} \leq (\mathbb{E} \|\widetilde{\Delta}_{jj}\|_{HS}^2 \mathbb{E} \|\widetilde{\Delta}_{kk}\|_{HS}^2)^{1/2} = O(n^{-1})$ by Cauchy-Schwarz inequality. It therefore follows that

$$\|\Gamma_1\|_{HS} = O_p \left(\frac{1}{\sqrt{pn}} + \frac{1}{\sqrt{n}} \right).$$

For Γ_2 , note that by Assumption 2.3 we have $\langle \boldsymbol{\Delta}, \boldsymbol{\varepsilon}_{\tau^*+1} - \boldsymbol{\varepsilon}_{\tau^*} \rangle_{L_p} = O_p(1)$ and $p^{-1} \|\boldsymbol{\Delta}\|_{L_p} = O_p(1)$. It follows that $\|\Gamma_2\|_{HS} = O_p(n^{-1})$, and then

$$(20) \quad \left\| \widehat{\mathcal{H}} - \mathcal{H} \right\|_{HS} = O_p \left(n^{-1/2} \right).$$

We emphasize that this result holds under both the null and the alternative hypotheses. Hence, by Lemmas 4.2 and 4.3 of [Bosq \(2000\)](#), it follows that for each $r = 1, \dots, R$, $|\widehat{\lambda}_r - \lambda_r| = o_p(1)$ and

$$(21) \quad \left\| \widehat{\psi}_r - \psi_r \right\|_{\mathcal{T}} \leq 2\sqrt{2}c_R^{-1} \left\| \widehat{\mathcal{H}} - \mathcal{H} \right\|_{HS},$$

where $c_R = \inf_{r=1, \dots, R} (\lambda_r - \lambda_{r+1})$, which implies that $\|\widehat{\psi}_r - \psi_r\|_{\mathcal{T}} = O_p(n^{-1/2})$.

We finally prove the element-wise convergence of $\widehat{\boldsymbol{\Sigma}}_r$. Define $\boldsymbol{\Delta}_i^\varepsilon = \{\Delta_i^\varepsilon(\mathbf{s}_1), \dots, \Delta_i^\varepsilon(\mathbf{s}_p)\}^T$ for $i = 1, \dots, n-1$, where $\Delta_i^\varepsilon(\mathbf{s}_j) = \varepsilon_{i+1}(\mathbf{s}_j) - \varepsilon_i(\mathbf{s}_j)$. Observe by (4) that

$$(22) \quad \begin{aligned}\widehat{\boldsymbol{\Sigma}}_r &= \frac{1}{2(n-1)} \sum_{i=1}^{n-1} \left\langle \boldsymbol{\Delta}_i^\varepsilon, \widehat{\psi}_r \right\rangle_{\mathcal{T}} \left\langle \boldsymbol{\Delta}_i^\varepsilon, \widehat{\psi}_r \right\rangle_{\mathcal{T}}^T - \frac{1}{2(n-1)} \left\langle \boldsymbol{\Delta}_{\tau^*}^\varepsilon, \widehat{\psi}_r \right\rangle_{\mathcal{T}} \left\langle \boldsymbol{\Delta}_{\tau^*}^\varepsilon, \widehat{\psi}_r \right\rangle_{\mathcal{T}}^T \\ &\quad + \frac{1}{2(n-1)} \left\langle (\mathbf{X}_{\tau^*+1} - \mathbf{X}_{\tau^*}), \widehat{\psi}_r \right\rangle_{\mathcal{T}} \left\langle (\mathbf{X}_{\tau^*+1} - \mathbf{X}_{\tau^*}), \widehat{\psi}_r \right\rangle_{\mathcal{T}}^T,\end{aligned}$$

and it can be shown that $\widehat{\boldsymbol{\Sigma}}_r(j, k) = \boldsymbol{\Theta}_1(j, k) + \boldsymbol{\Theta}_2(j, k) + \boldsymbol{\Theta}_3(j, k) + o_p(1)$ for each j, k , where

$$\boldsymbol{\Theta}_1 := \frac{1}{2(n-1)} \sum_{i=1}^{n-1} \left\langle \boldsymbol{\Delta}_i^\varepsilon, \psi_r \right\rangle_{\mathcal{T}} \left\langle \boldsymbol{\Delta}_i^\varepsilon, \psi_r \right\rangle_{\mathcal{T}}^T,$$

$$\Theta_2 := \frac{1}{2(n-1)} \sum_{i=1}^{n-1} \left\langle \Delta_i^\varepsilon, (\hat{\psi}_r - \psi_r) \right\rangle_{\mathcal{T}} \left\langle \Delta_i^\varepsilon, (\hat{\psi}_r - \psi_r) \right\rangle_{\mathcal{T}}^{\text{T}},$$

$$\Theta_3 := \frac{1}{(n-1)} \sum_{i=1}^{n-1} \left\langle \Delta_i^\varepsilon, \psi_r \right\rangle_{\mathcal{T}} \left\langle \Delta_i^\varepsilon, (\hat{\psi}_r - \psi_r) \right\rangle_{\mathcal{T}}^{\text{T}}.$$

Abbreviate $\Delta_i^\varepsilon(\mathbf{s}_j)$ as Δ_{ij}^ε for simplicity. For Θ_1 , the law of large numbers implies that $\Theta_1(j, k) \xrightarrow{P} \mathbb{E}\{\langle \Delta_{ij}^\varepsilon, \psi_r \rangle_{\mathcal{T}} \langle \Delta_{ik}^\varepsilon, \psi_r \rangle_{\mathcal{T}}\} / 2 = \sigma_r(\mathbf{s}_j, \mathbf{s}_k)$, since $\langle \Delta_{ij}^\varepsilon, \psi_r \rangle_{\mathcal{T}}$ forms a 1-dependent, mean-zero moving-average sequence in i with $\mathbb{E}\{\langle \Delta_{ij}^\varepsilon, \psi_r \rangle_{\mathcal{T}} \langle \Delta_{ik}^\varepsilon, \psi_r \rangle_{\mathcal{T}}\} = 2\mathbb{E}\{\xi_{ir}(\mathbf{s}_j) \xi_{ir}(\mathbf{s}_k)\}$. For Θ_2 , it follows from Cauchy–Schwarz inequality that $\Theta_2(j, k) \leq \frac{1}{2(n-1)} \sum_{i=1}^{n-1} \|\Delta_{ij}^\varepsilon\|_{\mathcal{T}} \|\Delta_{ik}^\varepsilon\|_{\mathcal{T}} \|\hat{\psi}_r - \psi_r\|_{\mathcal{T}}^2$, which implies that $\Theta_2(j, k) = o_p(1)$ by Assumption 2.3 and (21). Similarly we can derive that $\Theta_3(j, k) = o_p(1)$, which completes the proof for $\hat{\Sigma}_r(j, k) = \Sigma_r(j, k) + o_p(1)$.

B.2. Proof of Theorem 3.1. Recall the definitions that $\Sigma_r = \{\sigma_r(\mathbf{s}_j, \mathbf{s}_k)_{j,k=1,\dots,p}\}$, $P_r = \{\rho_r(\mathbf{s}_j, \mathbf{s}_k)_{j,k=1,\dots,p}\}$, and let $\xi_{ir}^* = (\xi_{ir,1}^*, \dots, \xi_{ir,p}^*)^{\text{T}}$ where $\xi_{ir,j}^* = \lambda_{r,j}^{-1/2} \xi_{ir}(\mathbf{s}_j)$. It follows from Lemma A.1 and the continuous mapping theorem that, for each $1 \leq r \leq R$,

$$n^{-1} \left(\sum_{1 \leq i \leq nx} \xi_{ir}^* - x \sum_{1 \leq i \leq n} \xi_{ir}^* \right)^{\text{T}} \mathbf{K}_h \left(\sum_{1 \leq i \leq nx} \xi_{ir}^* - x \sum_{1 \leq i \leq n} \xi_{ir}^* \right) \xrightarrow{d} \mathbf{B}_r^{\text{T}}(x) \mathbf{K}_h \mathbf{B}_r(x),$$

where $\mathbf{B}_r(\cdot) = \{B_{1r}(\cdot), \dots, B_{pr}(\cdot)\}^{\text{T}}$ is a p -dimensional Brownian bridge with covariance matrix P_r . Therefore, we have

$$(23) \quad \sum_{r=1}^R n^{-1} \left(\sum_{1 \leq i \leq nx} \xi_{ir}^* - x \sum_{1 \leq i \leq n} \xi_{ir}^* \right)^{\text{T}} \mathbf{K}_h \left(\sum_{1 \leq i \leq nx} \xi_{ir}^* - x \sum_{1 \leq i \leq n} \xi_{ir}^* \right) \\ \xrightarrow{d} \sum_{r=1}^R \mathbf{B}_r^{\text{T}}(x) \mathbf{K}_h \mathbf{B}_r(x),$$

Define that $\hat{\xi}_{ir}(\mathbf{s}_j) = \hat{\lambda}_{r,j}^{-1/2} \langle \varepsilon_i(\mathbf{s}_j), \hat{\psi}_r \rangle_{\mathcal{T}}$ and $\hat{\xi}_{ir} = \{\hat{\xi}_{ir}(\mathbf{s}_1), \dots, \hat{\xi}_{ir}(\mathbf{s}_p)\}^{\text{T}}$. We then study the impact of replacing ξ_{ir}^* in (23) by $\hat{\xi}_{ir}$. Note that under null hypothesis, we have

$$(24) \quad \hat{\eta}_{\tau,r}(\mathbf{s}_j) = \hat{\lambda}_{r,j}^{-1/2} \left\langle \hat{\Delta}_{\tau}(\mathbf{s}_j), \hat{\psi}_r \right\rangle_{\mathcal{T}} = \frac{1}{\sqrt{n}} \left\{ \sum_{i=1}^{\tau} \hat{\xi}_{ir}(\mathbf{s}_j) - \frac{\tau}{n} \sum_{i=1}^n \hat{\xi}_{ir}(\mathbf{s}_j) \right\}.$$

Let $\lambda_r = (\lambda_{r,1}, \dots, \lambda_{r,p})^{\text{T}}$, $\hat{\lambda}_r = (\hat{\lambda}_{r,1}, \dots, \hat{\lambda}_{r,p})^{\text{T}}$, and $\tilde{\varepsilon}_{i,r} = \{\lambda_{r,1}^{-1/2} \varepsilon_i(\mathbf{s}_1), \dots, \lambda_{r,p}^{-1/2} \varepsilon_i(\mathbf{s}_p)\}^{\text{T}}$. Observe that

$$\sup_{0 < x < 1} n^{-1/2} \left| \sum_{1 \leq i \leq nx} \hat{\xi}_{ir} - \sum_{1 \leq i \leq nx} \xi_{ir}^* \right| \\ = \sup_{0 < x < 1} n^{-1/2} \left| \sum_{1 \leq i \leq nx} \hat{\lambda}_r^{-1/2} \langle \varepsilon_i, \hat{\psi}_r \rangle - \sum_{1 \leq i \leq nx} \lambda_r^{-1/2} \langle \varepsilon_i, \psi_r \rangle \right| \\ \leq \sup_{0 < x < 1} \left| \left(\hat{\lambda}_r^{-1/2} - \lambda_r^{-1/2} \right) \left\langle n^{-1/2} \sum_{1 \leq i \leq nx} \varepsilon_i, \hat{\psi}_r \right\rangle \right|$$

$$+ \sup_{0 < x < 1} \left| \lambda_r^{-1/2} \left\langle n^{-1/2} \sum_{1 \leq i \leq nx} \boldsymbol{\varepsilon}_i, \hat{\boldsymbol{\psi}}_r - \boldsymbol{\psi}_r \right\rangle \right|,$$

where the first term is $o_p(1)$ due to the uniform consistency of $\hat{\boldsymbol{\lambda}}_r$ by Theorem 2.1 together with

$$(25) \quad \sup_{0 < x < 1} \left\| n^{-1/2} \sum_{1 \leq i \leq nx} \boldsymbol{\varepsilon}_i \right\|_p = O_p(1),$$

and the second term is $o_p(1)$ due to the l_2 consistency of $\hat{\boldsymbol{\psi}}_r$ in Theorem 2.1 together with

$$(26) \quad \sup_{0 < x < 1} \left\| n^{-1/2} \sum_{1 \leq i \leq nx} \tilde{\boldsymbol{\varepsilon}}_{i,r} \right\|_p = O_p(1).$$

Here equations (25) and (26) follow from Assumptions 2.3–2.4 and the weak convergence in $D^p\{[0, 1], L^2(\mathcal{T})\}$ of the partial sum processes $\sum_{1 \leq i \leq nx} \boldsymbol{\varepsilon}_i$ and $\sum_{1 \leq i \leq nx} \tilde{\boldsymbol{\varepsilon}}_{i,r}$. Consequently, we obtain the result that $\sup_{0 < x < 1} n^{-1/2} \left| \sum_{1 \leq i \leq nx} \hat{\boldsymbol{\xi}}_{ir} - \sum_{1 \leq i \leq nx} \boldsymbol{\xi}_{ir}^* \right| = o_p(1)$, which in turn implies that

$$(27) \quad \left\| \left(\sum_{1 \leq i \leq nx} \hat{\boldsymbol{\xi}}_{ir} - x \sum_{1 \leq i \leq n} \hat{\boldsymbol{\xi}}_{ir} \right) - \left(\sum_{1 \leq i \leq nx} \boldsymbol{\xi}_{ir}^* - x \sum_{1 \leq i \leq n} \boldsymbol{\xi}_{ir}^* \right) \right\|_p = o_p(n^{-1/2})$$

Combining (23) and (27), we have

$$(28) \quad \begin{aligned} & \sum_{r=1}^R n^{-1} \left(\sum_{1 \leq i \leq nx} \hat{\boldsymbol{\xi}}_{ir} - x \sum_{1 \leq i \leq n} \hat{\boldsymbol{\xi}}_{ir} \right)^\top \mathbf{K}_h \left(\sum_{1 \leq i \leq nx} \hat{\boldsymbol{\xi}}_{ir} - x \sum_{1 \leq i \leq n} \hat{\boldsymbol{\xi}}_{ir} \right) \\ & \xrightarrow{d} \sum_{r=1}^R \mathbf{B}_r^\top(x) \mathbf{K}_h \mathbf{B}_r(x), \end{aligned}$$

which completes the proof of Theorem 3.1.

B.3. Proof of Theorem 3.2. Let $\boldsymbol{\mu}_i = \{\mu_i(\mathbf{s}_1), \dots, \mu_i(\mathbf{s}_p)\}^\top$ and recall the definition of \mathbf{X}_i . Note that for $x \in (0, 1)$,

$$(29) \quad \sum_{1 \leq i \leq nx} \mathbf{X}_i - x \sum_{1 \leq i \leq n} \mathbf{X}_i = \left(\sum_{1 \leq i \leq nx} \boldsymbol{\varepsilon}_i - x \sum_{1 \leq i \leq n} \boldsymbol{\varepsilon}_i \right) + \left(\sum_{1 \leq i \leq nx} \boldsymbol{\mu}_i - x \sum_{1 \leq i \leq n} \boldsymbol{\mu}_i \right),$$

where the first term is $O_p(n^{1/2})$ by (25). Examining the second term we have

$$\sum_{1 \leq i \leq nx} \boldsymbol{\mu}_i - x \sum_{1 \leq i \leq n} \boldsymbol{\mu}_i = \begin{cases} nx(1 - \theta_0)\boldsymbol{\Delta}, & 0 < x \leq \theta_0, \\ n(1 - x)\theta_0\boldsymbol{\Delta}, & \theta_0 < x < 1, \end{cases}$$

where θ_0 and $\boldsymbol{\Delta}$ are defined in Section 3.2.

Define that $\hat{\boldsymbol{\eta}}_r(x) = \{\hat{\eta}_{r,1}(x), \dots, \hat{\eta}_{r,p}(x)\}^\top$ where $\hat{\eta}_{j,r}(x) = \hat{\lambda}_{r,j}^{-1/2} \langle \sum_{1 \leq i \leq nx} X_i(\mathbf{s}_j) - x \sum_{1 \leq i \leq n} X_i(\mathbf{s}_j), \hat{\boldsymbol{\psi}}_r \rangle_{\mathcal{T}} / \sqrt{n}$, and $\mathbf{D}_r = \text{diag}(\lambda_{r,1}^{-1/2}, \dots, \lambda_{r,p}^{-1/2})$. It then follows from Theorem 2.1, Slutsky's Theorem and functional continuous mapping theorem that for $0 < x \leq \theta_0$,

$$(30) \quad \hat{\boldsymbol{\eta}}_r(x) = \sqrt{nx}(1 - \theta_0)\mathbf{D}_r\boldsymbol{\Delta}_r + O_p(1),$$

which is uniformly true in $x \in (0, 1)$. Similarly, for $x > \theta_0$, we have

$$(31) \quad \hat{\boldsymbol{\eta}}_r(x) = \sqrt{n}\theta_0(1-x)\mathbf{D}_r\boldsymbol{\Delta}_r + O_p(1).$$

It then follows from (30) and (31) that

$$(32) \quad \sup_{0 < x < 1} \left| \frac{1}{n} \sum_{r=1}^R \hat{\boldsymbol{\eta}}_r^\top(x) \hat{\mathbf{D}}_r^\top \mathbf{K}_h \hat{\mathbf{D}}_r \hat{\boldsymbol{\eta}}_r(x) - g(x) \right| = o_p(1),$$

where $\hat{\mathbf{D}}_r = \text{diag}(\hat{\lambda}_{r,1}^{-1/2}, \dots, \hat{\lambda}_{r,p}^{-1/2})$ and

$$g(x) = \begin{cases} x^2(1-\theta_0)^2 \sum_{r=1}^R \boldsymbol{\Delta}_r^\top \mathbf{D}_r^\top \mathbf{K}_h \mathbf{D}_r \boldsymbol{\Delta}_r, & 0 < x \leq \theta_0, \\ \theta_0^2(1-x)^2 \sum_{r=1}^R \boldsymbol{\Delta}_r^\top \mathbf{D}_r^\top \mathbf{K}_h \mathbf{D}_r \boldsymbol{\Delta}_r, & \theta_0 < x < 1. \end{cases}$$

It then follows from Theorem 1 and the definition of $Q_h(\tau)$ that $n^{-1}Q_h^{max} = \sup_{0 < x < 1} g(x) + o_p(1)$, and the conclusion for Q_h^{sum} can be similarly obtained.

B.4. Proof of Corollary 3.1. Denote $\boldsymbol{\Gamma}_r = \mathbf{D}_r^\top \mathbf{K}_h \mathbf{D}_r$ and $\hat{\boldsymbol{\Gamma}}_r = \hat{\mathbf{D}}_r^\top \mathbf{K}_h \hat{\mathbf{D}}_r$. Under the Assumptions in Theorem 3.1, we have $g_R^* := \sum_{r=1}^R \boldsymbol{\Delta}_r^\top \boldsymbol{\Gamma}_r \boldsymbol{\Delta}_r > 0$, thus the continuous function $g(x)$ has a unique maximum at $x = \theta_0$. Then the uniform convergence in (32) implies that $|\hat{\tau}/n - \theta_0| = o_p(1)$ by noting the definition of $\hat{\tau}$. To further show $\hat{\tau} - \tau^* = O_p(1)$, we define that $Q_n(x) = \sum_{r=1}^R \hat{\boldsymbol{\eta}}_r^\top(x) \hat{\boldsymbol{\Gamma}}_r \hat{\boldsymbol{\eta}}_r(x)$, $\hat{\boldsymbol{\Delta}}_r = \langle \boldsymbol{\Delta}_r, \hat{\boldsymbol{\psi}}_r \rangle \boldsymbol{\tau}$ and $L_{n,\tau} = -(\tau^* - \tau)(\tau + \tau^*)(n - \tau^*)^2$. Following the similar arguments in the proof of Theorem 3.3(b) of [Ashton and Kirch \(2012\)](#) and noting that $\hat{\boldsymbol{\Gamma}}_r$ are symmetric matrices, we can obtain that for $\tau \leq \tau^*$, the decomposition of $Q_n(\tau/n) - Q_n(\tau^*/n)$ is dominated by $L_{n,\tau} \sum_{r=1}^R \hat{\boldsymbol{\Delta}}_r \hat{\boldsymbol{\Gamma}}_r \hat{\boldsymbol{\Delta}}_r = L_{n,\tau}(g_R^* + o_p(1))$ due to Theorem 2.1. As a result, it can be shown that for some large N ,

$$\begin{aligned} \Pr(\hat{\tau} \leq \tau^* - N) &= \Pr\left(\max_{\tau \leq \tau^* - N} Q_n(\tau/n) - Q_n(\tau^*/n) \geq \max_{\tau > \tau^* - N} Q_n(\tau/n) - Q_n(\tau^*/n)\right) \\ &\leq \Pr\left(\max_{\tau \leq \tau^* - N} Q_n(\tau/n) - Q_n(\tau^*/n) \geq 0\right) \\ &\leq \Pr\left((g_R^* + o_p(1)) \max_{\tau \leq \tau^* - N} L_{n,\tau} \geq 0\right) \rightarrow 0, \end{aligned}$$

as $g_R^* > 0$ and $\max_{\tau \leq \tau^* - N} L_{n,\tau} \leq -N\tau^*(n - \tau^*)^2 < 0$. Analogous arguments can be applied to show that $\Pr(\hat{\tau} \geq \tau^* + N) \rightarrow 0$, which completes the proof.

B.5. Proof of Theorem 4.1. To streamline the notation and avoid ambiguity, we omit the superscripts ‘‘O’’ and ‘‘E’’ in $\eta_{j,r}^{*O}$ and $\tilde{\eta}_{j,r}^{*E}$, yielding that $W_j^* = \sum_{r=1}^R \eta_{j,r}^* \tilde{\eta}_{j,r}^* = \boldsymbol{\eta}_j^{*\top} \tilde{\boldsymbol{\eta}}_j^*$. Similarly we abbreviate $\hat{\eta}_{\hat{\tau},r}^O(\mathbf{s}_j)$ and $\tilde{\eta}_{\hat{\tau},r}^E(\mathbf{s}_j)$ as $\hat{\eta}_{j,r}$ and $\tilde{\eta}_{j,r}$ for W_j , respectively. The first key result for the proof is the uniform symmetry property for W_j , i.e.,

$$(33) \quad \sup_{0 \leq t \leq t^*} \left| \frac{\sum_{j \in \mathcal{A}^c} \mathbb{I}(W_j \geq t)}{\sum_{j \in \mathcal{A}^c} \mathbb{I}(W_j \leq -t)} - 1 \right| = o_p(1)$$

with the upper bound t^* defined in (36). Note that Lemma A.1 provides the analogous symmetry property for W_j^* , where the proof is based on Lemmas C.3 and C.4. Meanwhile,

Lemma C.5 provides the uniform convergence for $\sum_{j \in \mathcal{A}^c} \mathbb{I}(W_j \geq t) / \sum_{j \in \mathcal{A}^c} \mathbb{I}(W_j^* \geq t)$ and $\sum_{j \in \mathcal{A}^c} \mathbb{I}(W_j \leq -t) / \sum_{j \in \mathcal{A}^c} \mathbb{I}(W_j^* \leq -t)$. Then the result in (33) follows by noticing

$$\begin{aligned} \left| \frac{\sum_{j \in \mathcal{A}^c} \mathbb{I}(W_j \geq t)}{\sum_{j \in \mathcal{A}^c} \mathbb{I}(W_j \leq -t)} - 1 \right| &\leq \left| \frac{\sum_{j \in \mathcal{A}^c} \mathbb{I}(W_j \geq t) - \sum_{j \in \mathcal{A}^c} \mathbb{I}(W_j^* \geq t)}{\sum_{j \in \mathcal{A}^c} \mathbb{I}(W_j \leq -t)} \right| \\ &+ \left| \left(\frac{\sum_{j \in \mathcal{A}^c} \mathbb{I}(W_j^* \geq t)}{\sum_{j \in \mathcal{A}^c} \mathbb{I}(W_j^* \leq -t)} - 1 \right) \cdot \frac{\sum_{j \in \mathcal{A}^c} \mathbb{I}(W_j^* \leq -t)}{\sum_{j \in \mathcal{A}^c} \mathbb{I}(W_j \leq -t)} \right| \\ &+ \left| \frac{\sum_{j \in \mathcal{A}^c} \mathbb{I}(W_j^* \leq -t)}{\sum_{j \in \mathcal{A}^c} \mathbb{I}(W_j \leq -t)} - 1 \right|. \end{aligned}$$

By definition, our thresholding rule is equivalent to select index j if $W_j \geq L$, where

$$L = \inf \left\{ t \geq 0 : 1 + \sum_j \mathbb{I}(W_j \leq -t) \leq \alpha \max \left(\sum_j \mathbb{I}(W_j \geq t), 1 \right) \right\}.$$

We need to establish an asymptotic bound for L such that (33) can be applied. Note that $\sum_{j \in \mathcal{A}^c} \mathbb{I}(W_j^* \leq -t^*) \approx \alpha b_p$ by (40), where $A_n \approx B_n$ denotes that $A_n/B_n \xrightarrow{p} 1$. By Lemmas C.5 and C.6, one then obtains that

$$\sum_j \mathbb{I}(W_j < -t^*) \approx \sum_{j \in \mathcal{A}^c} \mathbb{I}(W_j \leq -t^*) \approx \sum_{j \in \mathcal{A}^c} \mathbb{I}(W_j^* \leq -t^*) \approx \alpha b_p \lesssim \alpha \sum_j \mathbb{I}(W_j > t^*),$$

where $A_n \lesssim B_n$ means $\Pr(A_n \leq B_n) \rightarrow 1$. Hence,

$$(34) \quad \Pr(0 \leq L \leq t^*) \rightarrow 1,$$

and consequently,

$$(35) \quad \frac{\sum_{j \in \mathcal{A}^c} \mathbb{I}(W_j \geq L)}{\sum_{j \in \mathcal{A}^c} \mathbb{I}(W_j \leq -L)} \xrightarrow{p} 1.$$

Finally, by the definition of FDP and the selection rule of L , we have

$$\begin{aligned} \text{FDP}_w(L) &= \frac{\sum_{j \in \mathcal{A}^c} \mathbb{I}(W_j \geq L)}{1 \vee \sum_j \mathbb{I}(W_j \geq L)} = \frac{\sum_j \mathbb{I}(W_j \leq -L)}{1 \vee \sum_j \mathbb{I}(W_j \geq L)} \times \frac{\sum_{j \in \mathcal{A}^c} \mathbb{I}(W_j \geq L)}{\sum_j \mathbb{I}(W_j \leq -L)} \\ &\leq \alpha \times \frac{\sum_{j \in \mathcal{A}^c} \mathbb{I}(W_j \geq L)}{\sum_{j \in \mathcal{A}^c} \mathbb{I}(W_j \leq -L)}, \end{aligned}$$

which completes the proof for $\limsup_{n,p \rightarrow \infty} \text{FDP}_w(L) \leq \alpha$ due to (35).

B.6. Proof of Corollary 4.1. This corollary is a direct conclusion derived from the proof of Theorem 4.1. Combining (34) and (49), we have

$$\Pr(W_j > L, \text{ for any } j \in \beta_p) \geq \Pr(W_j > t^*, \text{ for any } j \in \beta_p) \rightarrow 1,$$

which completes the proof.

APPENDIX C: ADDITIONAL LEMMAS

The first is the standard Hoeffding's inequality for sub-Gaussian variables, and the second is a moderate deviation result provided in [Cao \(2007\)](#).

LEMMA C.1. *Let $\{X_i\}_{i=1}^n$ be independent centered sub-Gaussian random variables with parameter γ_i^2 , i.e. $\mathbb{E}\{\exp(s X_i)\} \leq \exp(s^2 \gamma_i^2/2)$ for any $s \in \mathbb{R}$. Then for any $\epsilon > 0$, we have*

$$\Pr\left(\left|\sum_{i=1}^n X_i\right| > \epsilon\right) \leq 2 \exp\left(\frac{-\epsilon^2}{2 \sum_{i=1}^n \gamma_i^2}\right).$$

LEMMA C.2. *Let X_1, \dots, X_{n_1} be a sample of i.i.d. random variables with mean μ_1 and variance σ_1^2 , and Y_1, \dots, Y_{n_2} be another sample of i.i.d. random variables with mean μ_2 and variance σ_2^2 that is independent of $\{X_i, 1 \leq i \leq n_1\}$. Denote T as the two-sample t -statistic $T = \frac{\bar{X} - \bar{Y} - (\mu_1 - \mu_2)}{\sqrt{\sigma_1^2/n_1 + \sigma_2^2/n_2}}$. Assume that $\mathbb{E}|X_1|^3 < \infty$, $\mathbb{E}|Y_1|^3 < \infty$ and that there exists $0 < c_1 < c_2 < \infty$ such that $c_1 < n_1/n_2 < c_2$. Then*

$$\frac{\Pr(T \geq x)}{1 - \Phi(x)} \rightarrow 1$$

uniformly in $x \in (0, o((n_1 + n_2)^{1/6}))$.

Define $G(t) := p_0^{-1} \sum_{j \in \mathcal{A}^c} \Pr(W_j^* \geq t | \mathcal{X}_E)$ and $G_-(t) := p_0^{-1} \sum_{j \in \mathcal{A}^c} \Pr(W_j^* \leq -t | \mathcal{X}_E)$, where $p_0 = |\mathcal{A}^c|$ denote the cardinality of null set. For any function F , let $F^{-1}(y) := \inf\{t \geq 0 : F(t) \leq y\}$. Then set

$$(36) \quad t^* = G_-^{-1}(\alpha b_p / p_0),$$

where b_p is defined in Assumption 4.3. Lemma C.3 characterizes the symmetry property between $G(t)$ and $G_-(t)$.

LEMMA C.3. *Suppose Assumptions 2.4 and 4.1–4.2 hold. Then we have*

$$\frac{G(t)}{G_-(t)} - 1 \rightarrow 0$$

uniformly for all $t \in [0, t^*]$.

Lemma C.4 establishes the uniform convergence of $\sum_{j \in \mathcal{A}^c} \mathbb{I}(W_j^* \geq t) / p_0 G(t)$ and $\sum_{j \in \mathcal{A}^c} \mathbb{I}(W_j^* \leq -t) / p_0 G_-(t)$,

LEMMA C.4. *Suppose Assumptions 2.4, 4.2 and 4.4 hold. Then conditional on \mathcal{X}_E ,*

$$(37) \quad \begin{aligned} \sup_{0 \leq t \leq t^*} \left| \frac{\sum_{j \in \mathcal{A}^c} \mathbb{I}(W_j^* \geq t)}{p_0 G(t)} - 1 \right| &= o_p(1), \\ \sup_{0 \leq t \leq t^*} \left| \frac{\sum_{j \in \mathcal{A}^c} \mathbb{I}(W_j^* \leq -t)}{p_0 G_-(t)} - 1 \right| &= o_p(1). \end{aligned}$$

Lemma C.5 provides the uniform convergence of $\sum_{j \in \mathcal{A}^c} \mathbb{I}(W_j \geq t) / \sum_{j \in \mathcal{A}^c} \mathbb{I}(W_j^* \geq t)$ and $\sum_{j \in \mathcal{A}^c} \mathbb{I}(W_j \leq -t) / \sum_{j \in \mathcal{A}^c} \mathbb{I}(W_j^* \leq -t)$.

LEMMA C.5. *Suppose Assumptions 2.1–2.4, 4.1–4.2 and 4.4–4.5 hold, then*

$$\sup_{0 \leq t \leq t^*} \left| \frac{\sum_{j \in \mathcal{A}^c} \mathbb{I}(W_j \geq t)}{\sum_{j \in \mathcal{A}^c} \mathbb{I}(W_j^* \geq t)} - 1 \right| = o_p(1),$$

$$\sup_{0 \leq t \leq t^*} \left| \frac{\sum_{j \in \mathcal{A}^c} \mathbb{I}(W_j \leq -t)}{\sum_{j \in \mathcal{A}^c} \mathbb{I}(W_j^* \leq -t)} - 1 \right| = o_p(1).$$

Lemma C.6 further implies that, with probability tending to 1, $\sum_j \mathbb{I}(W_j > t^*)$ is larger than b_p , where b_p denotes the minimum number of identifiable effect sizes.

LEMMA C.6. *Suppose Assumptions 2.1–2.4, 4.2–4.3 and 4.5 hold, then*

$$\Pr \left(\sum_j \mathbb{I}(W_j > t^*) \geq b_p \right) \rightarrow 1.$$

APPENDIX D: PROOFS FOR THE LEMMAS

D.1. Proof of Lemmas A.1–A.4.

PROOF OF LEMMA A.1. Note that under the weak separability structure in Section 2.1, we have $\text{cov}\{\xi_{ir}(\mathbf{s}_j), \xi_{i'r'}(\mathbf{s}_k)\} = \mathbb{I}(i = i')\mathbb{I}(r = r')\sigma_r(\mathbf{s}_j, \mathbf{s}_k)$. Then the result in Lemma A.1 follows directly from the functional central limit theorem (e.g. Bosq, 2000) with respect to the Skorokhod space $D^{pR}[0, 1]$. \square

PROOF OF LEMMA A.2. (a) This result follows immediately from the fact that the uncorrelatedness of $\eta_{j,r}^*$ across r and by the direct calculation

$$\text{var}(\eta_{j,r}^*) = \text{var} \left\{ \frac{\tau^*(n - \tau^*)}{n\sqrt{n}} \left(\frac{1}{\tau^*} \sum_{i=1}^{\tau^*} \xi_{ir,j}^* - \frac{1}{n - \tau^*} \sum_{i=\tau^*+1}^n \xi_{ir,j}^* \right) \right\} = \theta_0(1 - \theta_0)(1 - 2\theta_0).$$

(b) We shall show that the assertion holds for each $\eta_{j,r}^*$ and $\delta_{j,r}^*$ with some large $C_\eta > 0$, i.e.

$$\Pr \left(\left| \eta_{j,r}^* - \sqrt{n}\theta_0(1 - \theta_0)\delta_{j,r}^* \right| > \sqrt{C_\eta \log p} \right) = o(1/p),$$

and the case for η_j^* is straightforward by using the Bonferroni inequality since R is fixed. For each r , define that $Z_{ij,r} = (1 - \theta_0)\xi_{ir,j}^*$ for $i \leq \tau^*$ and $Z_{ij,r} = -\theta_0\xi_{ir,j}^*$ for $i > \tau^*$. By definition, we have $\eta_{j,r}^* - \sqrt{n}\theta_0(1 - \theta_0)\delta_{j,r}^* = n^{-1/2} \sum_{i=1}^n Z_{ij,r}$, and thus it suffices to show that $\Pr \left(\left| \sum_{i=1}^n Z_{ij,r} \right| > \sqrt{C_\eta n \log p} \right) = o(1/p)$ for each j and r . This can be obtained directly from Lemma C.1 and Assumption 4.2 with

$$(38) \quad \Pr \left(\left| \sum_{i=1}^n Z_{ij} \right| > \sqrt{C_\eta n \log p} \right) \leq 2 \exp \left(\frac{-C_\eta \log p}{2c\gamma^2} \right) = o(1/p),$$

where $c = \min\{\theta_0^2, (1 - \theta_0)^2\}$.

To prove the result for $\tilde{\eta}_j^*$, we denote $\boldsymbol{\xi}_j^* = (\xi_{j,1}^*, \dots, \xi_{j,R}^*)^\top$ where $\xi_{j,r}^* = \frac{1}{\tau^*} \sum_{i=1}^{\tau^*} \xi_{ir,j}^* - \frac{1}{n - \tau^*} \sum_{i=\tau^*+1}^n \xi_{ir,j}^*$, and $w_{k,j} = K_h(\mathbf{s}_k - \mathbf{s}_j) / \sum_k K_h(\mathbf{s}_k - \mathbf{s}_j)$ for each j . By definition, we

then have $\boldsymbol{\eta}_j^* = \sqrt{n}\theta_0(1 - \theta_0) \left(\boldsymbol{\delta}_j^* + \boldsymbol{\xi}_j^* \right)$, $\tilde{\boldsymbol{\eta}}_j^* = \sqrt{n}\theta_0(1 - \theta_0) \sum_k w_{k,j} (\boldsymbol{\delta}_k^* + \boldsymbol{\xi}_k^*)$, and

$$\begin{aligned} \|\tilde{\boldsymbol{\eta}}_j^* - \boldsymbol{\eta}_j^*\| &\leq \sqrt{n}\theta_0(1 - \theta_0) \left(\left\| \sum_k w_{k,j} (\boldsymbol{\delta}_k^* - \boldsymbol{\delta}_j^*) \right\| + \left\| \sum_k w_{k,j} (\boldsymbol{\xi}_k^* - \boldsymbol{\xi}_j^*) \right\| \right) \\ &\leq \sqrt{n}\theta_0(1 - \theta_0) \left(\max_{k:|k-j|\leq h} \|\boldsymbol{\delta}_k^* - \boldsymbol{\delta}_j^*\| + \max_k (\|\boldsymbol{\xi}_k^*\| + \|\boldsymbol{\xi}_j^*\|) \right), \end{aligned}$$

It then follows from Assumption 4.5 and the same argument in (38) that

$$(39) \quad \Pr \left(\|\tilde{\boldsymbol{\eta}}_j^* - \boldsymbol{\eta}_j^*\| > \sqrt{C \log p} \right) = o(1/p)$$

for some large C , which consequently implies that

$$\Pr \left(\|\tilde{\boldsymbol{\eta}}_j^* - \sqrt{n}\theta_0(1 - \theta_0)\boldsymbol{\delta}_j^*\| > \sqrt{C \log p} \right) = o(1/p).$$

□

PROOF OF LEMMA A.3. The asymptotic symmetry result in Lemma A.3 follows directly from Lemmas C.3 and C.4. Hence, it remains only to show that $t^* \leq C_\eta \log p$. According to the definition of t^* and Lemma C.4,

$$(40) \quad \alpha b_p/p_0 = G_-(t^*) = \frac{1}{p_0} \sum_{j \in \mathcal{A}^c} \mathbb{I}(W_j^* \leq -t^*) \{1 + o(1)\}.$$

On the other hand, it follows from Lemma A.2(b) that

$$\begin{aligned} &\Pr \left(\sum_{j \in \mathcal{A}^c} \mathbb{I}(W_j^* \leq -C_\eta \log p) > 0 \right) \\ &\leq \sum_{j \in \mathcal{A}^c} \Pr(W_j^* \leq -C_\eta \log p) \\ &\leq \sum_{j \in \mathcal{A}^c} \Pr(\|\boldsymbol{\eta}_j^*\| \|\tilde{\boldsymbol{\eta}}_j^*\| \geq C_\eta \log p) \\ &\leq \sum_{j \in \mathcal{A}^c} \Pr(\|\tilde{\boldsymbol{\eta}}_j^*\| > \sqrt{C_\eta \log p}) + \sum_{j \in \mathcal{A}^c} \Pr(\|\boldsymbol{\eta}_j^*\| > \sqrt{C_\eta \log p}) = o(1), \end{aligned}$$

which implies $\Pr \left(\sum_{j \in \mathcal{A}^c} \mathbb{I}(W_j^* \leq -C_\eta \log p) = 0 \right) \rightarrow 1$. Hence combining with (40), one obtains $t^* \leq C_\eta \log p$. □

PROOF OF LEMMA A.4. (a) Applying the similar arguments as in the proof of Theorem 4 in Zapata, Oh and Petersen (2022), we have

$$\Pr \left(\|\hat{\mathcal{H}} - \mathcal{H}\|_{HS} \geq \epsilon \right) \leq C'_2 \exp(-C'_1 \varpi_r^{-2} n \epsilon^2),$$

and

$$\Pr \left(\|\hat{\mathcal{C}}_{jj} - \mathcal{C}_{jj}\|_{HS} \geq \epsilon \right) \leq C'_2 \exp(-C'_1 \varpi_r^{-2} n \epsilon^2),$$

where $\varpi_1 = 2\sqrt{2}(\lambda_1 - \lambda_2)^{-1}$ and $\varpi_r = 2\sqrt{2} \max\{(\lambda_{r-1} - \lambda_r)^{-1}, (\lambda_r - \lambda_{r+1})^{-1}\}$ for $r \geq 2$. Moreover, applying the result (S4) in Zapata, Oh and Petersen (2022), for each $j = 1, \dots, p$,

$$|\hat{\lambda}_{r,j} - \lambda_{r,j}| \leq 2M\varpi_r \|\hat{\mathcal{H}} - \mathcal{H}\|_{HS} + \|\hat{\mathcal{C}}_{jj} - \mathcal{C}_{jj}\|_{HS},$$

Therefore, we can obtain the concentration inequality

$$(41) \quad \Pr \left(\left| \hat{\lambda}_{r,j} - \lambda_{r,j} \right| \geq \epsilon \right) \leq C_2 \exp \left(-C_1 \varpi_r^{-2} n \epsilon^2 \right),$$

It then follows that for any $c > 1$,

$$\begin{aligned} \Pr \left(\max_j \left| \hat{\lambda}_{r,j} - \lambda_{r,j} \right| \geq \sqrt{\frac{c \log p}{n}} \right) &\leq \sum_j \Pr \left(\left| \hat{\lambda}_{r,j} - \lambda_{r,j} \right| \geq \sqrt{\frac{c \log p}{n}} \right) \\ &\leq Cp \exp(-c \log p) = o(1), \end{aligned}$$

which implies that

$$\max_j \left| \hat{\lambda}_{r,j}^{-1/2} - \lambda_{r,j}^{-1/2} \right| = \max_j \left| \frac{\hat{\lambda}_{r,j} - \lambda_{r,j}}{\hat{\lambda}_{r,j}^{-1/2} \lambda_{r,j}^{-1/2} (\hat{\lambda}_{r,j}^{-1/2} + \lambda_{r,j}^{-1/2})} \right| = O_p \left((\log p/n)^{1/2} \right).$$

(b) Assume that $\hat{\tau} \leq \tau^*$ w.l.o.g., we have

$$\begin{aligned} &\left| \left\langle \widehat{\Delta}_{\hat{\tau}}(\mathbf{s}_j) - \widehat{\Delta}_{\tau^*}(\mathbf{s}_j), \psi_r \right\rangle_{\mathcal{T}} \right| \\ &= \frac{1}{\sqrt{n}} \left| \left\langle \left(\sum_{i=1}^{\hat{\tau}} X_i(\mathbf{s}_j) - \frac{\hat{\tau}}{n} \sum_{i=1}^n X_i(\mathbf{s}_j) \right) - \left(\sum_{i=1}^{\tau^*} X_i(\mathbf{s}_j) - \frac{\tau^*}{n} \sum_{i=1}^n X_i(\mathbf{s}_j) \right), \psi_r \right\rangle_{\mathcal{T}} \right| \\ &\leq \frac{1}{\sqrt{n}} \left| \left\langle \sum_{i=\hat{\tau}+1}^{\tau^*} X_i(\mathbf{s}_j), \psi_r \right\rangle_{\mathcal{T}} \right| + \frac{\tau^* - \hat{\tau}}{n\sqrt{n}} \left| \left\langle \sum_{i=1}^n X_i(\mathbf{s}_j), \psi_r \right\rangle_{\mathcal{T}} \right| \\ &= \frac{1}{\sqrt{n}} \left| \sum_{i=\hat{\tau}+1}^{\tau^*} \{ \mu_{ir}(\mathbf{s}_j) + \xi_{ir}(\mathbf{s}_j) \} \right| + \frac{\tau^* - \hat{\tau}}{n\sqrt{n}} \left| \sum_{i=1}^n \{ \mu_{ir}(\mathbf{s}_j) + \xi_{ir}(\mathbf{s}_j) \} \right| := W_{j1} + W_{j2} \end{aligned}$$

where $\mu_{ir}(\mathbf{s}_j) = \langle \mu_i(\mathbf{s}_j), \psi_r \rangle_{\mathcal{T}}$. Note that $\tau^* - \hat{\tau} = O_p(1)$ by Corollary 3.1, applying Lemma C.1 to $\xi_{ir}(\mathbf{s}_j)$ under Assumption 4.2, we have

$$\Pr \left(\left| \sum_{i=\hat{\tau}+1}^{\tau^*} \xi_{ir}(\mathbf{s}_j) \right| > \sqrt{C \log p} \right) \leq 2 \exp \left(\frac{-C_{\tau} \log p}{2(\tau^* - \hat{\tau})M\gamma^2} \right) = o(1/p)$$

for some large constant C_{τ} , and

$$(42) \quad \Pr \left(\left| \sum_{i=1}^n \xi_{ir}(\mathbf{s}_j) \right| > \sqrt{Cn \log p} \right) \leq 2 \exp \left(\frac{-C \log p}{2M\gamma^2} \right) = o(1/p),$$

which implies $\Pr(\max_j \left| \sum_{i=\hat{\tau}+1}^{\tau^*} \xi_{ir}(\mathbf{s}_j) \right| > \sqrt{C \log p}) = o(1)$ and $\Pr(\max_j \left| \sum_{i=1}^n \xi_{ir}(\mathbf{s}_j) \right| > \sqrt{Cn \log p}) = o(1)$, respectively. It then follows that

$$\max_j W_{j1} = O_p \left((\log p/n)^{1/2} \right) \text{ and } \max_j W_{j2} = O_p \left(\sqrt{\log p/n} \right),$$

provided that the mean function $\boldsymbol{\mu}_i(\cdot)$ is uniformly bounded, which yields the result in (b).

(c) Recall that $\eta_{j,r}^* = \lambda_{r,j}^{-1/2} \langle \widehat{\Delta}_{\tau^*}(\mathbf{s}_j), \psi_r \rangle_{\mathcal{T}}$ and $\hat{\eta}_{j,r} = \hat{\lambda}_{r,j}^{-1/2} \langle \widehat{\Delta}_{\hat{\tau}}(\mathbf{s}_j), \psi_r \rangle_{\mathcal{T}}$, where for notation simplicity we write $\Delta_{\tau^*,j} := \Delta_{\tau^*}(\mathbf{s}_j)$ and $\Delta_{\hat{\tau},j} := \Delta_{\hat{\tau}}(\mathbf{s}_j)$. Moreover, we omit the

subscripts “ r ” in $\hat{\eta}_{j,r}$, $\eta_{j,r}^*$, $\delta_{j,r}^*$ and $\lambda_{r,j}$, and “ \mathcal{T} ” in $\langle \cdot, \cdot \rangle_{\mathcal{T}}$ without confusion. For each $j = 1, \dots, p$, we have

$$\begin{aligned} |\hat{\eta}_j - \eta_j^*| &= \lambda_j^{-1/2} \left| \left\langle \widehat{\Delta}_{\hat{\tau}}(\mathbf{s}_j) - \widehat{\Delta}_{\tau^*}(\mathbf{s}_j), \psi_r \right\rangle \right| + \lambda_j^{-1/2} \left| \left\langle \widehat{\Delta}_{\hat{\tau}}(\mathbf{s}_j), \hat{\psi}_r - \psi_r \right\rangle \right| \\ &\quad + \left| \left(\hat{\lambda}_j^{-1/2} - \lambda_j^{-1/2} \right) \left\langle \widehat{\Delta}_{\hat{\tau}}(\mathbf{s}_j), \hat{\psi}_r \right\rangle \right| := L_{j1} + L_{j2} + L_{j3} \end{aligned}$$

According to Lemma A.4(b), $\max_j L_{j1} = O_p((\log p/n)^{1/2})$ since λ_j is uniformly bounded from Assumptions 2.4 and 4.2. To obtain the order for L_{j2} and L_{j3} , we first show that for any $j \in \mathcal{A}_h^c$,

$$(43) \quad \Pr \left(\left| \left\langle \widehat{\Delta}_{\tau^*}(\mathbf{s}_j), \psi_r \right\rangle \right| > \sqrt{C_1 \log p} \right) = o(1/p),$$

and

$$(44) \quad \Pr \left(\left| \left\langle \widehat{\Delta}_{\tau^*}(\mathbf{s}_j), \hat{\psi}_r \right\rangle \right| > \sqrt{C_1 \log p} \right) = o(1/p),$$

for some large C_1 . Note that $\langle \widehat{\Delta}_{\tau^*}(\mathbf{s}_j), \psi_r \rangle = \sqrt{n} \theta_0 (1 - \theta_0) \lambda_j \delta_j^* + n^{-1/2} \{ \sum_{i=1}^{\tau^*} \xi_{ir}(\mathbf{s}_j) - \frac{\tau^*}{n} \sum_{i=1}^n \xi_{ir}(\mathbf{s}_j) \}$. Then (43) follows by Assumption 4.5 and that $\Pr(|\sum_{i=1}^{\tau^*} \xi_{ir}(\mathbf{s}_j) - \frac{\tau^*}{n} \sum_{i=1}^n \xi_{ir}(\mathbf{s}_j)| > \sqrt{C_1 n \log p}) = o(1/p)$, which can be shown using similar arguments as (42). To obtain (44), we further show that

$$(45) \quad \Pr \left(\left| \left\langle \widehat{\Delta}_{\tau^*}(\mathbf{s}_j), \hat{\psi}_r - \psi_r \right\rangle \right| > \frac{C_2 \log p}{\sqrt{n}} \right) = o(1/p),$$

for some large C_2 . Note that $\max_j \mathbb{E} \|\widehat{\Delta}_{\tau^*}(\mathbf{s}_j)\|^2 \leq M_1$ for some large constant M_1 that depends on M specified in Assumption 4.2, and the similar arguments for (42) yield

$$\Pr \left(\|\hat{\psi}_r - \psi_r\| > \sqrt{\frac{C \log p}{n}} \right) = o(1/p).$$

Then (45) follows by applying Cauchy–Schwarz inequality, which leads to $\max_j L_{j2} = O_p(\log p/n^{1/2})$ based on Lemma A.4(b). Similarly, we can obtain $\max_j L_{j3} = O_p(\log p/n^{1/2})$ from (44) and Lemma A.4(a), which completes the proof for $\max_{j \in \mathcal{A}_h^c} |\hat{\eta}_j - \eta_j^*| = O_p(\log p/n^{1/2})$.

(d) Observe that $|W_j - W_j^*| \leq \sum_{r=1}^R |\hat{\eta}_{j,r}(\tilde{\eta}_{j,r} - \tilde{\eta}_{j,r}^*) + \tilde{\eta}_{j,r}^*(\hat{\eta}_{j,r} - \eta_{j,r}^*)|$. For each $r = 1, \dots, R$, it follows from Lemma A.4(c) that

$$(I.1) \quad \max_{j \in \mathcal{A}^c} |\hat{\eta}_{j,r} - \eta_{j,r}^*| = O_p(\log p/n^{1/2}),$$

and

$$(I.2) \quad \max_{j \in \mathcal{A}^c} |\tilde{\eta}_{j,r} - \tilde{\eta}_{j,r}^*| \leq \max_{j \in \mathcal{A}_h^c} |\hat{\eta}_{k,r} - \eta_{k,r}^*| = O_p(\log p/n^{1/2}).$$

On the other hand, it follows from Lemma A.2(b) that

$$\Pr \left(\max_{j \in \mathcal{A}^c} |\eta_{j,r}^*| > \sqrt{C_\eta \log p} \right) \leq \sum_{j \in \mathcal{A}^c} \Pr \left(|\eta_{j,r}^*| > \sqrt{C_\eta \log p} \right) = o(1),$$

which implies that $\max_{j \in \mathcal{A}^c} |\eta_{j,r}^*| = O_p((\log p)^{1/2})$. Therefore,

$$(I.3) \quad \max_{j \in \mathcal{A}^c} |\hat{\eta}_{j,r}| \leq \max_{j \in \mathcal{A}^c} |\hat{\eta}_{j,r} - \eta_{j,r}^*| + \max_{j \in \mathcal{A}^c} |\eta_{j,r}^*| = O_p((\log p)^{1/2}),$$

and

$$(I.4) \quad \max_{j \in \mathcal{A}^c} |\tilde{\eta}_{j,r}^*| \leq \max_{j \in \mathcal{A}^c} |\eta_{j,r}^*| + \max_{j \in \mathcal{A}^c} |\tilde{\eta}_{j,r}^* - \eta_{j,r}^*| = O_p \left((\log p)^{1/2} \right),$$

where $\max_{j \in \mathcal{A}^c} |\tilde{\eta}_{j,r}^* - \eta_{j,r}^*| = O_p \left((\log p)^{1/2} \right)$ is due to (39) in the proof of Lemma A.2(b). Combining (I.1)-(I.4), we conclude that

$$(46) \quad \max_{j \in \mathcal{A}^c} |W_j^* - W_j| = O_p \left((\log p)^{3/2} / n^{1/2} \right) = o_p \left((\log p)^{-1/2} \right)$$

by Assumption 4.1. \square

D.2. Proof of Lemmas C.3-C.6.

PROOF OF LEMMA C.3. By the definitions of W_j^* , $G(t)$ and $G_-(t)$, we have

$$G(t)/G_-(t) - 1 = \{p_0 G_-(t)\}^{-1} \sum_{j \in \mathcal{A}^c} \tilde{P}_j(t),$$

where $\tilde{P}_j(t) = \Pr \left(\boldsymbol{\eta}_j^{*\text{T}} \tilde{\boldsymbol{\eta}}_j^* \geq t | \mathcal{X}_E \right) - \Pr \left(\boldsymbol{\eta}_j^{*\text{T}} \tilde{\boldsymbol{\eta}}_j^* \leq -t | \mathcal{X}_E \right)$. On one hand, for $\mathcal{A}_t := \{j : \|\tilde{\boldsymbol{\eta}}_j^*\| < t / \sqrt{C_\eta \log p}\}$ where C_η is a large constant specified in Lemma A.2(b), we have

$$\begin{aligned} \frac{\sum_{j \in \mathcal{A}^c \cap \mathcal{A}_t} \tilde{P}_j(t)}{p_0 G_-(t)} &\leq \frac{\sum_{j \in \mathcal{A}^c} \Pr \left(\boldsymbol{\eta}_j^{*\text{T}} \tilde{\boldsymbol{\eta}}_j^* \geq t | \mathcal{X}_E \right)}{p_0 G_-(t)} \\ &\leq \frac{\sum_{j \in \mathcal{A}^c} \Pr \left(\|\boldsymbol{\eta}_j^*\| \geq \sqrt{C_\eta \log p} | \mathcal{X}_E \right)}{\alpha b_p} = o(1), \end{aligned}$$

where the second inequality follows immediately from the fact that $G_-(t)$ is decreasing and $t \leq G_-^{-1}(\alpha b_p / p_0)$.

On the other hand, for the case $\|\tilde{\boldsymbol{\eta}}_j^*\| \geq t / \sqrt{C_\eta \log p}$, we note that for $j \in \mathcal{A}^c$,

$$\boldsymbol{\eta}_j^{*\text{T}} \tilde{\boldsymbol{\eta}}_j^* = \frac{1}{\sqrt{n}} \left(\sum_{i=1}^{\tau^*} \boldsymbol{\xi}_{i,j}^{*\text{T}} \tilde{\boldsymbol{\eta}}_j^* - \frac{\tau^*}{n} \sum_{i=1}^n \boldsymbol{\xi}_{i,j}^{*\text{T}} \tilde{\boldsymbol{\eta}}_j^* \right),$$

where $\boldsymbol{\xi}_{i,j}^* = (\xi_{i1,j}^*, \dots, \xi_{iR,j}^*)^\text{T}$. Denote $\tilde{\boldsymbol{\eta}}_j^* = \mathbf{u}$ given \mathcal{X}_E , we can derive that $\mathbb{E}(\boldsymbol{\eta}_j^{*\text{T}} \mathbf{u} | \mathcal{X}_E) = 0$ and $\text{cov}(\boldsymbol{\eta}_j^{*\text{T}} \mathbf{u} | \mathcal{X}_E) = \mathbf{u}^\text{T} \boldsymbol{\Sigma}_j^* \mathbf{u}$, where $\boldsymbol{\Sigma}_j^*$ is defined in Lemma A.2(a). It then follows by Lemma C.2 and Assumptions 4.1–4.2 that

$$\Pr \left(\boldsymbol{\eta}_j^{*\text{T}} \tilde{\boldsymbol{\eta}}_j^* \geq t | \mathcal{X}_E \right) = \{1 - \Phi(t / \mathbf{u}^\text{T} \boldsymbol{\Sigma}_j^* \mathbf{u})\} \{1 + o_p(1)\},$$

where $o_p(1)$ is uniformly in j . Similarly, we can obtain that $\Pr(\boldsymbol{\eta}_j^{*\text{T}} \tilde{\boldsymbol{\eta}}_j^* \leq -t | \mathcal{X}_E) = \Phi(-t / \mathbf{u}^\text{T} \boldsymbol{\Sigma}_j^* \mathbf{u}) \{1 + o_p(1)\}$. It then follows that $\sum_{j \in \mathcal{A}^c \cap \mathcal{A}_t^c} \tilde{P}_j(t) = o(1)$, which leads to that $G(t)/G_-(t) - 1 = o(1)$ by combining the result for $j \in \mathcal{A}_t$. \square

PROOF OF LEMMA C.4. We only prove the first formula, and the second one holds similarly. Note that $G(t)$ is a decreasing and continuous function. Following the discretization approach in Du et al. (2021), we let $z_0 < z_1 < \dots < z_{h_n} \leq 1$ and $t_i = G^{-1}(z_i)$, where $z_0 = a_p / p_0$, $a_p = \alpha b_p$, $z_i = a_p / p_0 + w_p \exp(i^\zeta) / p_0$, $h_n = \{\log((p_0 - a_p) / w_p)\}^{1/\zeta}$ with

$w_p/a_p \rightarrow 0$ and $0 < \zeta < 1$. Note that $G(t_i)/G(t_{i+1}) = 1 + o(1)$ uniformly in i . It is therefore enough to derive the convergence rate of

$$D_n = \sup_{0 \leq i \leq h_n} \left| \frac{\sum_{j \in \mathcal{A}^c} \left\{ \mathbb{I}(W_j^* > t_i) - \Pr(W_j^* > t_i | \mathcal{X}_E) \right\}}{p_0 G(t_i)} \right|.$$

Define that

$$\begin{aligned} D(t) &:= \mathbb{E} \left[\left(\sum_{j \in \mathcal{A}^c} \left\{ \mathbb{I}(W_j^* > t) - \Pr(W_j^* > t | \mathcal{X}_E) \right\} \right)^2 \middle| \mathcal{X}_E \right] \\ &= \sum_{j \in \mathcal{A}^c} \sum_{k \in \mathcal{A}^c} \left\{ \Pr(W_j^* > t, W_k^* > t | \mathcal{X}_E) - \Pr(W_k^* > t | \mathcal{X}_E) \Pr(W_j^* > t | \mathcal{X}_E) \right\}, \end{aligned}$$

and $\mathcal{M}_j = \{k \in \mathcal{A}^c : |\sum_{r=1}^R \rho_r(\mathbf{s}_j, \mathbf{s}_k)| \geq C_\rho (\log n)^{-2-\nu}\}$, where C_ρ and ν are defined in Assumption 4.4. It then follows that

$$(47) \quad \begin{aligned} D(t) &\leq l_p p_0 G(t) + \sum_{j \in \mathcal{A}^c} \sum_{k \in \mathcal{M}_j^c} \left\{ \Pr(W_k^* > t, W_j^* > t | \mathcal{X}_E) \right. \\ &\quad \left. - \Pr(W_k^* > t | \mathcal{X}_E) \Pr(W_j^* > t | \mathcal{X}_E) \right\}. \end{aligned}$$

For the second term of the right-hand side of (47), we notice that for $j \in \mathcal{A}^c$ and $k \in \mathcal{M}_j^c$,

$$\left| \frac{\text{cov} \left\{ (W_j^*, W_k^*) \middle| \mathcal{X}_E \right\}}{\sqrt{\text{var}(W_j^* | \mathcal{X}_E) \text{var}(W_k^* | \mathcal{X}_E)}} \right| \leq C (\log n)^{-2-\nu}$$

for some constant C depend on C_ρ and θ_0 . To see this, denote $\tilde{\eta}_{j,r}^* = u_{j,r}$ given \mathcal{X}_E . For each $j \in \mathcal{A}^c$ and $k \in \mathcal{M}_j^c$, it follows from Lemma A.2(a) that

$$\begin{aligned} \text{var}(W_j^* | \mathcal{X}_E) &= \sum_{r=1}^R \text{var}(\eta_{j,r}^* u_{j,r}) = \theta_0 (1 - \theta_0) (1 - 2\theta_0) \sum_{r=1}^R u_{j,r}^2, \\ \text{cov} \left\{ (W_j^*, W_k^*) \middle| \mathcal{X}_E \right\} &= \sum_{r=1}^R u_{j,r} u_{k,r} \text{cov}(\eta_{j,r}^*, \eta_{k,r}^*) = c_{\theta_0} \sum_{r=1}^R u_{j,r} u_{k,r} \rho_r(\mathbf{s}_j, \mathbf{s}_k), \end{aligned}$$

where $c_{\theta_0} > 0$ is some constant depends on θ_0 . Consequently, applying Lemma 1 in Cai and Liu (2016) we obtain that

$$\left| \frac{\Pr(W_k^* > t, W_j^* > t | \mathcal{X}_E) - \Pr(W_k^* > t | \mathcal{X}_E) \Pr(W_j^* > t | \mathcal{X}_E)}{\Pr(W_k^* > t | \mathcal{X}_E) \Pr(W_j^* > t | \mathcal{X}_E)} \right| \leq (\log n)^{-1-\nu_1}$$

uniformly holds, where $\nu_1 = \min(\nu, 1/2)$. It then follows from (47) that

$$(48) \quad \begin{aligned} \Pr(D_n \geq \epsilon | \mathcal{X}_E) &\leq \sum_{i=0}^{h_n} \Pr \left(\left| \frac{\sum_{j \in \mathcal{A}^c} \left[\mathbb{I}(W_j^* > t_i) - \Pr(W_j^* > t_i | \mathcal{X}_E) \right]}{p_0 G(t_i)} \right| \geq \epsilon \right) \\ &\leq \frac{1}{\epsilon^2} \sum_{i=0}^{h_n} \frac{D(t_i)}{p_0^2 G^2(t_i)} \leq \frac{1}{\epsilon^2} \left\{ l_p \sum_{i=0}^{h_n} \frac{1}{p_0 G(t_i)} + h_n (\log n)^{-1-\nu_1} \right\}. \end{aligned}$$

Observing that

$$\sum_{i=0}^{h_n} \frac{1}{p_0 G(t_i)} = \frac{1}{a_p} + \sum_{i=1}^{h_n} \frac{1}{a_p + w_p e^{i\zeta}} \leq w_p^{-1} \{1 + O(1)\},$$

we can then conclude that $D_n = o_p(1)$ when $l_p/b_p \rightarrow 0$ by noting that (a) ζ can be arbitrarily close to 1 such that $h_n(\log n)^{-1-\nu_1} \rightarrow 0$, and (b) w_p can be made arbitrarily large as long as $w_p/a_p \rightarrow 0$. This completes the proof of (C.4). \square

PROOF OF LEMMA C.5. Note that the result in Lemma C.4 implies that for any $\epsilon > 0$,

$$\sup_{0 \leq t \leq t^*} \Pr \left(\left| \frac{\sum_{j \in \mathcal{A}^c} \mathbb{I}(W_j^* \geq t)}{p_0 G(t)} - 1 \right| \geq \epsilon \right) = o(1),$$

$$\int_0^{t^*} \Pr \left(\left| \frac{\sum_{j \in \mathcal{A}^c} \mathbb{I}(W_j^* \geq t)}{p_0 G(t)} - 1 \right| \geq \epsilon \right) dt = o(t^*/h_n).$$

Then, it follows from (46) and the arguments in the proof of Theorem 3.1 in Liu (2013) that

$$\sup_{0 \leq t \leq t^*} \left| \frac{\sum_{j \in \mathcal{A}^c} \mathbb{I}(W_j \geq t)}{p_0 G(t)} - 1 \right| = o_p(1),$$

which is a counterpart of (37) based on W_j . Then the first equation in Lemma C.5 can be obtained using again (37), and the second follows similarly. \square

PROOF OF LEMMA C.6. We first show that for each $j \in \beta_p$, $\Pr(W_j^* \leq C_\eta \log p) = o(1/p)$. According to the proof of Lemma A.2(b), we have $\boldsymbol{\eta}_j^* = \sqrt{n}\theta_* (\boldsymbol{\delta}_j^* + \boldsymbol{\xi}_j^*)$ and $\tilde{\boldsymbol{\eta}}_j^* = \sqrt{n}\theta_* \sum_k w_{k,j} (\boldsymbol{\delta}_k^* + \boldsymbol{\xi}_k^*)$, where $\theta_* := \theta_0(1 - \theta_0)$. Then for each $j \in \beta_p$,

$$\begin{aligned} & \Pr(W_j^* \leq C_\eta \log p) \\ & \leq \Pr \left(n\theta_*^2 \sum_k w_{k,j} \left(\boldsymbol{\delta}_j^{*\top} \boldsymbol{\delta}_k^* + \boldsymbol{\delta}_j^{*\top} \boldsymbol{\xi}_k^* + \boldsymbol{\xi}_j^{*\top} \boldsymbol{\delta}_k^* + \boldsymbol{\xi}_j^{*\top} \boldsymbol{\xi}_k^* \right) \leq C_\eta \log p \right) \\ & = \Pr \left(\sum_k w_{k,j} \left(\boldsymbol{\delta}_j^{*\top} \boldsymbol{\xi}_k^* + \boldsymbol{\xi}_j^{*\top} \boldsymbol{\delta}_k^* + \boldsymbol{\xi}_j^{*\top} \boldsymbol{\xi}_k^* \right) \leq \frac{C_\eta \log p}{n\theta_*^2} - \sum_k w_{k,j} \boldsymbol{\delta}_j^{*\top} \boldsymbol{\delta}_k^* \right) \\ & \leq \Pr \left(\sum_k w_{k,j} \left(\|\boldsymbol{\delta}_j^*\| \|\boldsymbol{\xi}_k^*\| + \|\boldsymbol{\xi}_j^*\| \|\boldsymbol{\delta}_k^*\| + \|\boldsymbol{\xi}_j^*\| \|\boldsymbol{\xi}_k^*\| \right) \geq \sum_k w_{k,j} \boldsymbol{\delta}_j^{*\top} \boldsymbol{\delta}_k^* - \frac{C_\eta \log p}{n\theta_*^2} \right), \end{aligned}$$

where the last inequality is due to Cauchy–Schwarz inequality. Define $d_j = \sum_k w_{k,j} \boldsymbol{\delta}_j^{*\top} \boldsymbol{\delta}_k^* - C_\eta \log p / n\theta_*^2$. Then it suffices to show that

$$\Pr \left(\sum_k w_{k,j} \|\boldsymbol{\delta}_j^*\| \|\boldsymbol{\xi}_k^*\| \geq \frac{d_j}{3}, j \in \beta_p \right) = o(1/p),$$

and similar results for other two terms regarding $\|\boldsymbol{\xi}_j^*\| \|\boldsymbol{\delta}_k^*\|$ and $\|\boldsymbol{\xi}_j^*\| \|\boldsymbol{\xi}_k^*\|$ can be easily obtained. Note that $\Pr(\max_k \|\boldsymbol{\xi}_k^*\| \geq C\sqrt{\log p/n}) = o(1/p)$ by the proof in Lemma A.2(b), it then suffices to show $\sqrt{n}d_j / (\|\boldsymbol{\delta}_j^*\| \sqrt{\log p}) \rightarrow \infty$ for any $j \in \beta_p$. To see this,

$$\begin{aligned} \frac{\sqrt{n}d_j}{\|\boldsymbol{\delta}_j^*\| \sqrt{\log p}} & \geq \frac{\sqrt{n} \sum_k w_{k,j} \boldsymbol{\delta}_j^{*\top} (\boldsymbol{\delta}_k^* + \boldsymbol{\delta}_k^* - \boldsymbol{\delta}_j^*)}{\|\boldsymbol{\delta}_j^*\| \sqrt{\log p}} - \frac{C_\eta \sqrt{\log p}}{\theta_*^2 \|\boldsymbol{\delta}_j^*\| \sqrt{n}} \\ & \geq \frac{\sqrt{n} \|\boldsymbol{\delta}_j^*\|}{\sqrt{\log p}} - \frac{\sqrt{n} \max_{k \in \beta_p^*} \|\boldsymbol{\delta}_k^* - \boldsymbol{\delta}_j^*\|}{\sqrt{\log p}} - \frac{C_\eta \sqrt{\log p}}{\theta_*^2 \|\boldsymbol{\delta}_j^*\| \sqrt{n}} \rightarrow \infty \end{aligned}$$

as $n, p \rightarrow \infty$ by Assumptions 4.3 and 4.5, where $\beta_p^h = \beta_p \cup \{k : |k - j| \leq h \text{ where } j \in \beta_p\}$. Therefore, we conclude that $\Pr(W_j^* \leq C_\eta \log p) = o(1/p)$ for each $j \in \beta_p$, and similarly $\Pr(W_j \leq C_\eta \log p) = o(1/p)$ using similar arguments for proving (46) and Lemma A.4(c). Since $t^* \leq C_\eta \log p$, it then follows that

$$(49) \quad \Pr(W_j \leq t^*, \text{ for some } j \in \beta_p) \leq \sum_{j \in \beta_p} \Pr(W_j \leq t^*) \rightarrow 0,$$

and consequently,

$$\Pr\left(\sum_j \mathbb{I}(W_j > t^*) \geq b_p\right) \geq \Pr\left(\sum_{j \in \beta_p} \mathbb{I}(W_j > t^*) \geq b_p\right) \rightarrow 1.$$

□

APPENDIX E: ADDITIONAL NUMERICAL RESULTS

E.1. additional simulation results. First, we analyze the simulation results for the case $n = 200$. Table 6 presents the empirical power results for $n = 200$ under various spatial signal scenarios, with the highest power in each scenario highlighted in bold, and Figure 5 reports the multiple testing results for $p = 50, 100$, and 200 with $n = 200$. It is evident that, as the sample size increases, both the change-point detection and support recovery procedures exhibit substantially higher power compared to the $n = 100$ case. Meanwhile, the results of empirical FDR remain similar to those in the main paper, where our methods still outperform competing approaches. Additionally, Table 7 assesses the performance of the proposed change-point estimation approach in terms of the mean and standard deviation when $r_s = 0.6$ and $n = 100$. Q_h exhibits the smallest estimation errors across nearly all settings.

Next, we investigate the effect of varying spatial covariance on the performance of the change-point detection and support-recovery procedures. By adjusting the range parameter ϕ_1 , we control the degree of spatial dependence, with larger values of ϕ_1 indicating stronger spatial correlation. Table 8 reports the empirical size under different levels of spatial dependence. For $n = 100$ and $p = 100$, all methods except $\hat{\Lambda}_2$ maintain empirical size close to the nominal level, regardless of the strength of spatial dependence. Table 9 presents the empirical power results under various scenarios of spatial correlations, with the highest power in each scenario highlighted in bold. Although the power gradually decreases with increasing spatial dependence, our method Q_h maintains superior detection power across all correlation levels. Figure 6 illustrates the impact of varying spatial correlation on FDR and average power. We observe that fSDA exhibits slightly inflated FDR beyond the nominal level under strong spatial correlation with weak signals, while still demonstrating substantially higher power than competing methods. Furthermore, LAWS fails to maintain proper FDR control, whereas the remaining two methods show relatively conservative performance.

E.2. additional empirical data results. To evaluate the space-time separability structure of the considered dataset, we perform hypothesis testing based on the strong separability test proposed by Aston et al. (2017) and the weak separability test from Luo, Zhang and Liang (2025). Both tests are appropriate for replicated spatiotemporal functional data, with the latter also applicable for assessing the partial separability of multivariate functional data. To account for potential mean shifts in the precipitation data, the cross-covariance estimation in both tests is adapted by using the estimated mean functions defined in (17), for the years before and after the change-point, rather than the typical sample mean function for all years. The test result provided in Table 10 shows clear evidence for rejecting the hypothesis

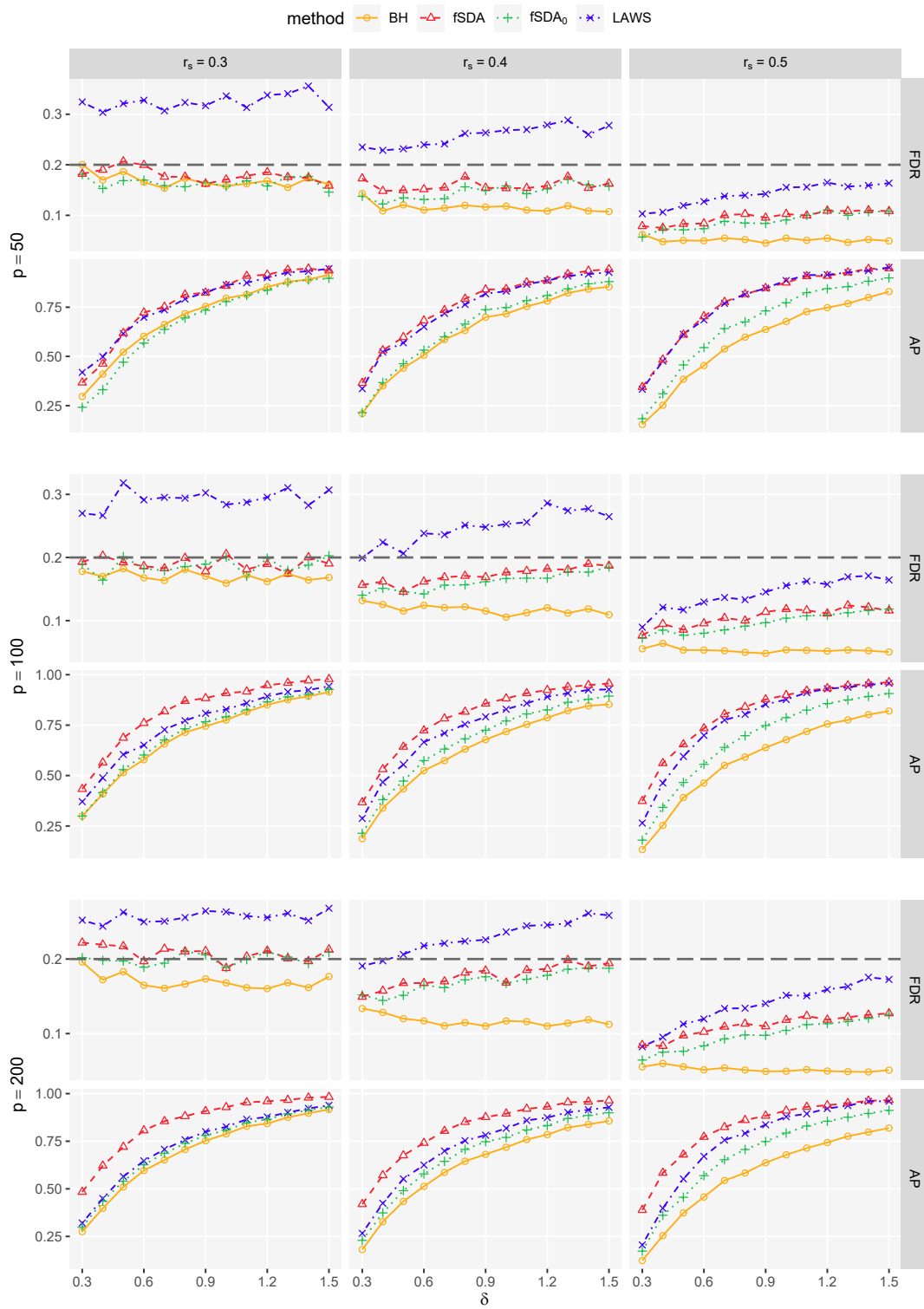


FIG 5. FDR and AP comparison for varying r_s with $n = 200$. The dashed line represents the nominal level $\alpha = 0.2$.

TABLE 6
Empirical power (%) of the change-point tests using various methods with $n = 200$.

Method	Type	$r_s = 0.4$			$r_s = 0.6$			
		$\delta = 0.2$	$\delta = 0.3$	$\delta = 0.4$	$\delta = 0.2$	$\delta = 0.3$	$\delta = 0.4$	
$p = 20$	Q_0	sum	16.5	36.5	51.5	14.5	28.0	60.0
		max	10.5	21.5	38.5	8.0	15.5	45.0
	Q_h	sum	21.5	36.5	55.0	19.0	51.0	73.5
		max	15.0	37.5	55.0	17.5	48.0	74.0
	Gro	$\widehat{\Lambda}_1$	17.0	34.0	53.0	15.0	27.5	61.5
		$\widehat{\Lambda}_2$	10.5	17.5	29.5	12.5	14.0	28.5
$p = 50$	Q_0	sum	27.0	42.0	76.5	24.5	47.0	79.5
		max	14.5	24.5	51.5	13.0	26.5	63.0
	Q_h	sum	32.5	58.0	81.5	43.5	79.5	90.5
		max	30.0	52.0	77.0	37.0	74.5	91.0
	Gro	$\widehat{\Lambda}_1$	27.0	46.0	76.5	28.0	48.0	80.5
		$\widehat{\Lambda}_2$	20.0	25.5	36.0	16.0	27.5	42.0
$p = 100$	Q_0	sum	42.5	74.0	94.0	49.5	93.0	100
		max	42.0	57.5	72.5	42.0	95.5	100
	Q_h	sum	65.5	93.0	97.5	76.5	95.5	100
		max	60.5	93.5	97.0	77.0	95.0	100
	Gro	$\widehat{\Lambda}_1$	46.0	72.5	92.5	56.0	92.5	100
		$\widehat{\Lambda}_2$	26.5	43.0	59.0	31.0	59.0	86.0

TABLE 7
Simulation study on the consistency of the change-point detection procedures with the mean and standard deviation (in parentheses) of $|\widehat{\tau} - \tau^*|$'s under different settings with $r_s = 0.6$ and $n = 100$.

Method	$\delta = 0.4$			$\delta = 1$		
	$p = 20$	$p = 50$	$p = 100$	$p = 20$	$p = 50$	$p = 100$
Q_0	3.57(3.71)	2.13 (2.56)	2.02(2.44)	0.52(1.04)	0.18(0.48)	0.05(0.24)
Q_h	3.49 (3.69)	2.17(2.55)	1.74 (2.27)	0.51 (1.01)	0.17 (0.46)	0.04 (0.23)
$\widehat{\Lambda}_1$	4.25(3.91)	2.68(3.05)	2.62(2.84)	0.55(1.17)	0.20(0.57)	0.06(0.27)
$\widehat{\Lambda}_2$	5.34(5.12)	4.64(4.51)	4.20(4.13)	1.41(2.37)	0.69(1.18)	0.27(0.59)

TABLE 8
Empirical size (%) of the change-point tests with different ϕ_1 .

Method	Type	$n = 100, p = 100$		
		$\phi_1 = 0.1$	$\phi_1 = 0.15$	$\phi_1 = 0.2$
Q_0	sum	4.5	5.7	5.2
	max	4.4	5.3	3.2
Q_h	sum	5.5	5.0	4.7
	max	6.2	6.3	5.2
Gro	$\widehat{\Lambda}_1$	5.7	6.3	4.3
	$\widehat{\Lambda}_2$	9.8	9.3	9.2

of strong separability. However, the assumption of weak separability is not rejected across different FVE levels, which provides adequate support for the subsequent functional change-point modeling approach.

TABLE 9
Empirical power (%) of the change-point tests with different ϕ_1 when $n = 100, p = 100$.

Method	Type	$\delta = 0.2$			$\delta = 0.4$			
		$\phi_1 = 0.1$	$\phi_1 = 0.15$	$\phi_1 = 0.2$	$\phi_1 = 0.1$	$\phi_1 = 0.15$	$\phi_1 = 0.2$	
$r_s = 0.4$	Q_0	sum	24.5	15.5	14.0	79.5	80.0	70.5
		max	14.0	12.0	10.5	80.0	72.5	63.0
	Q_h	sum	36.0	22.5	15.5	91.5	83.5	65.0
		max	30.0	16.0	9.5	92.0	79.5	53.0
	Gro	$\widehat{\Lambda}_1$	22.5	13.5	10.0	78.0	63.0	48.0
		$\widehat{\Lambda}_2$	19.5	15.0	15.5	42.0	30.5	26.0

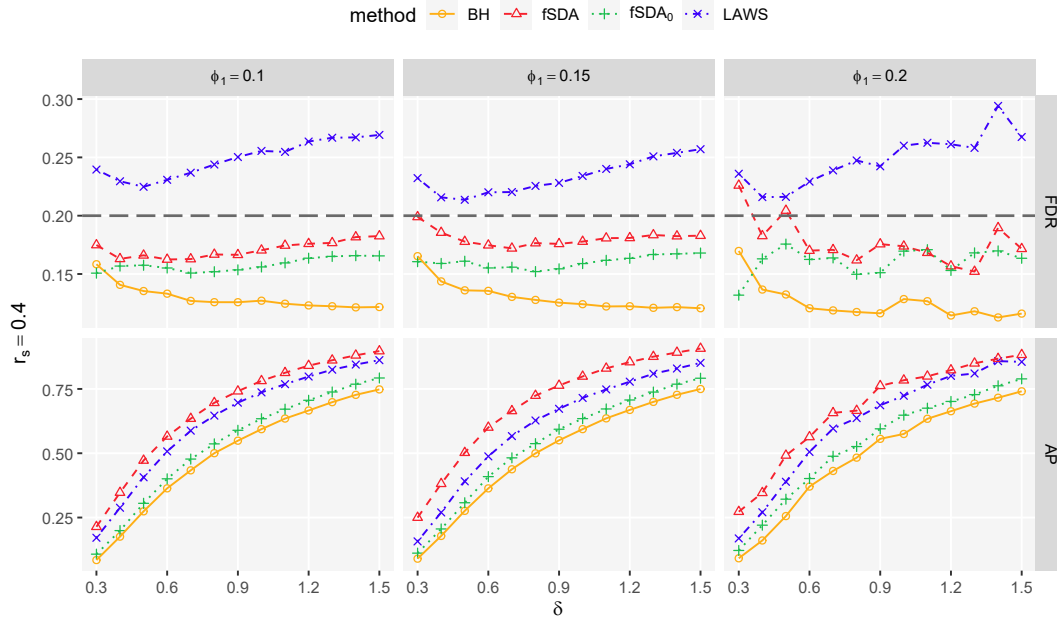


FIG 6. FDR and AP comparison for varying ϕ_1 with $n = 100, p = 100$. The dashed line represents the nominal level $\alpha = 0.2$.

TABLE 10
The p -values of different types of separability tests for China precipitation data.

weak separability			strong separability
FVE=80%	FVE=90%	FVE=95%	
0.402	0.286	0.253	0.016

Figure 7 visualizes the function $Q_h(\tau)$ across different τ values, indicating that the estimated change-year for China’s precipitation data is $\hat{\tau} = 1988$.

REFERENCES

ASTON, J. A. and KIRCH, C. (2012). Detecting and estimating changes in dependent functional data. *Journal of Multivariate Analysis* **109** 204–220.
 ASTON, J. A., PIGOLI, D., TAVAKOLI, S. et al. (2017). Tests for separability in nonparametric covariance operators of random surfaces. *The Annals of Statistics* **45** 1431–1461.

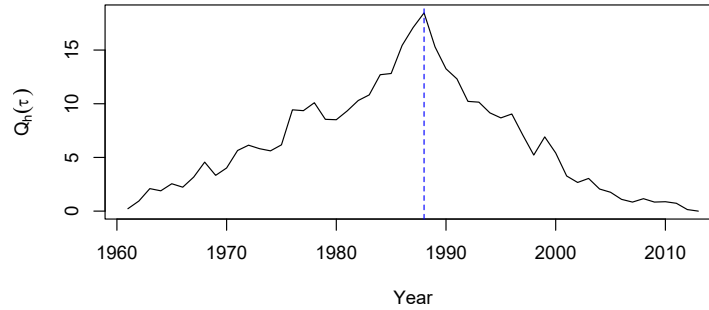


FIG 7. The function $Q_h(\tau)$ against $1961 \leq \tau \leq 2013$ with the dashed line marking the estimated change-point.

- AUE, A., RICE, G. and SÖNMEZ, O. (2018). Detecting and dating structural breaks in functional data without dimension reduction. *Journal of the Royal Statistical Society Series B: Statistical Methodology* **80** 509–529.
- BARBER, R. F. and CANDÈS, E. J. (2015). Controlling the false discovery rate via knockoffs. *The Annals of Statistics* **43** 2055–2085.
- BENJAMINI, Y. and HELLER, R. (2007). False discovery rates for spatial signals. *Journal of the American Statistical Association* **102** 1272–1281.
- BENJAMINI, Y. and HOCHBERG, Y. (1995). Controlling the false discovery rate: a practical and powerful approach to multiple testing. *Journal of the Royal Statistical Society Series B: Statistical Methodology* **57** 289–300.
- BENJAMINI, Y. and YEKUTIELI, D. (2001). The control of the false discovery rate in multiple testing under dependency. *Annals of statistics* 1165–1188.
- BERKES, I., GABRYS, R., HORVÁTH, L. and KOKOSZKA, P. (2009). Detecting changes in the mean of functional observations. *Journal of the Royal Statistical Society Series B: Statistical Methodology* **71** 927–946.
- BOSQ, D. (2000). *Linear processes in function spaces: theory and applications*. Springer Science & Business Media.
- BROWN, D. A., LAZAR, N. A., DATTA, G. S., JANG, W. and MCDOWELL, J. E. (2014). Incorporating spatial dependence into Bayesian multiple testing of statistical parametric maps in functional neuroimaging. *NeuroImage* **84** 97–112.
- BRUNSELL, N. A. (2010). A multiscale information theory approach to assess spatial-temporal variability of daily precipitation. *Journal of Hydrology* **385** 165–172.
- CAI, T. T. and LIU, W. (2016). Large-scale multiple testing of correlations. *Journal of the American Statistical Association* **111** 229–240.
- CAI, T. T., SUN, W. and XIA, Y. (2022). LAWS: A locally adaptive weighting and screening approach to spatial multiple testing. *Journal of the American Statistical Association* **117** 1370–1383.
- CAO, H. (2007). Moderate deviations for two sample t -statistics. *ESAIM: Probability and Statistics* **11** 264–271.
- CAO, H. and WU, W. (2015). Changepoint estimation: another look at multiple testing problems. *Biometrika* **102** 974–980.
- CHEN, H., REN, H., YAO, F. and ZOU, C. (2023). Data-driven selection of the number of change-points via error rate control. *Journal of the American Statistical Association* **118** 1415–1428.
- CRESSIE, N. and WIKLE, C. K. (2011). *Statistics for spatio-temporal data*. John Wiley & Sons.
- DU, L., GUO, X., SUN, W. and ZOU, C. (2021). False discovery rate control under general dependence by symmetrized data aggregation. *Journal of the American Statistical Association* **118** 607–621.
- GAO, L., BANERJEE, S. and RITZ, B. (2023). Spatial difference boundary detection for multiple outcomes using Bayesian disease mapping. *Biostatistics* **24** 922–944.
- GROMENKO, O., KOKOSZKA, P. and REIMHERR, M. (2017). Detection of change in the spatiotemporal mean function. *Journal of the Royal Statistical Society Series B: Statistical Methodology* **79** 29–50.
- HÖRMANN, S., KOKOSZKA, P. et al. (2010). Weakly dependent functional data. *The Annals of Statistics* **38** 1845–1884.
- HORVÁTH, L. and KOKOSZKA, P. (2012). *Inference for functional data with applications*. Springer Science & Business Media.

- HSING, T. and EUBANK, R. (2015). *Theoretical foundations of functional data analysis, with an introduction to linear operators*. John Wiley & Sons.
- KONER, S. and STAIKU, A.-M. (2023). Second-generation functional data. *Annual review of statistics and its application* **10** 547–572.
- LI, D., LI, R. and SHANG, H. L. (2024). Detection and estimation of structural breaks in high-dimensional functional time series. *The Annals of Statistics* **52** 1716–1740.
- LI, B., ZHANG, X. and SMERDON, J. E. (2016). Comparison between spatio-temporal random processes and application to climate model data. *Environmetrics* **27** 267–279.
- LIANG, D., HUANG, H., GUAN, Y. and YAO, F. (2023). Test of weak separability for spatially stationary functional field. *Journal of the American Statistical Association* **118** 1606–1619.
- LIU, W. (2013). Gaussian graphical model estimation with false discovery rate control. *The Annals of Statistics* **41** 2948–2978.
- LIU, C., RAY, S. and HOOKER, G. (2017). Functional principal component analysis of spatially correlated data. *Statistics and Computing* **27** 1639–1654.
- LIU, W. and SHAO, Q.-M. (2014). Phase transition and regularized bootstrap in large-scale t -tests with false discovery rate control. *The Annals of Statistics* **42** 2003–2025.
- LIU, M., LIU, P., GUO, Y., WANG, Y., GENG, X., NIE, Z. and YU, Y. (2019). Change-point analysis of precipitation and drought extremes in china over the past 50 years. *Atmosphere* **11** 11.
- LUO, F., ZHANG, W. and LIANG, D. (2025). Test of partial separability for multivariate functional data. *Statistica Sinica* published online.
- NG, C.-P., ZHANG, Q. and LI, W. (2021). Changes in hourly extreme precipitation over Eastern China from 1970 to 2019 dominated by synoptic-scale precipitation. *Geophysical Research Letters* **48** e2020GL090620.
- PACIFICO, M. P., GENOVESE, C., VERDINELLI, I. and WASSERMAN, L. (2004). False discovery control for random fields. *Journal of the American Statistical Association* **99** 1002–1014.
- PAYNABAR, K., ZOU, C. and QIU, P. (2016). A change-point approach for phase-I analysis in multivariate profile monitoring and diagnosis. *Technometrics* **58** 191–204.
- REN, H., ZOU, C., CHEN, N. and LI, R. (2022). Large-scale datastreams surveillance via pattern-oriented-sampling. *Journal of the American Statistical Association* **117** 794–808.
- RISSE, M. D., PACIOREK, C. J. and STONE, D. A. (2019). Spatially dependent multiple testing under model misspecification, with application to detection of anthropogenic influence on extreme climate events. *Journal of the American Statistical Association* **114** 61–78.
- SUN, W., REICH, B. J., TONY CAI, T., GUINDANI, M. and SCHWARTZMAN, A. (2015). False discovery control in large-scale spatial multiple testing. *Journal of the Royal Statistical Society Series B: Statistical Methodology* **77** 59–83.
- WANG, J.-L., CHIOU, J.-M. and MÜLLER, H.-G. (2016). Functional data analysis. *Annual Review of Statistics and its application* **3** 257–295.
- WANG, G. and FENG, L. (2023). Computationally efficient and data-adaptive changepoint inference in high dimension. *Journal of the Royal Statistical Society Series B: Statistical Methodology* **85** 936–958.
- YAN, H., PAYNABAR, K. and SHI, J. (2018). Real-time monitoring of high-dimensional functional data streams via spatio-temporal smooth sparse decomposition. *Technometrics* **60** 181–197.
- YUN, Z. X., SOOIN and BO, L. (2022). Detection of local differences in spatial characteristics between two spatiotemporal random fields. *Journal of the American Statistical Association* **117** 291–306.
- ZAPATA, J., OH, S.-Y. and PETERSEN, A. (2022). Partial separability and functional graphical models for multivariate Gaussian processes. *Biometrika* **109** 665–681.
- ZHANG, H. and LI, Y. (2022). Unified principal component analysis for sparse and dense functional data under spatial dependency. *Journal of Business & Economic Statistics* **40** 1523–1537.
- ZHANG, H., ZHU, Z. and YIN, S. (2019). Identifying precipitation regimes in China using model-based clustering of spatial functional data. *arXiv preprint arXiv:1904.10152*.
- ZHANG, X., SHAO, X., HAYHOE, K. and WUEBBLES, D. J. (2011). Testing the structural stability of temporally dependent functional observations and application to climate projections. *Electronic Journal of Statistics* **5** 1765–1796.